





RESEARCH ARTICLE

Downregulated expression of lactate dehydrogenase in adult oligodendrocytes and its implication for the transfer of glycolysis products to axons

Erik Späte¹ | Baoyu Zhou¹ | Ting Sun^{1,2} | Kathrin Kusch^{1,3}  |
 Ebrahim Asadollahi¹ | Sophie B. Siems¹ | Constanze Depp¹ | Hauke B. Werner¹ |
 Gesine Saher¹  | Johannes Hirrlinger^{1,4}  | Wiebke Möbius¹ |
 Klaus-Armin Nave¹ | Sandra Goebbels¹ 

¹Department of Neurogenetics, Max Planck Institute for Multidisciplinary Sciences, Göttingen, Germany

²Laboratory of Molecular Neurobiology, Department of Biochemistry and Biophysics, Karolinska Institutet, Stockholm, Sweden

³Institute for Auditory Neuroscience and InnerEarLab, University Medical Center Göttingen, Göttingen, Germany

⁴Carl-Ludwig-Institute for Physiology, Faculty of Medicine, Leipzig University, Leipzig, Germany

Correspondence

Sandra Goebbels and Klaus-Armin Nave, Department of Neurogenetics, Max Planck Institute for Multidisciplinary Sciences, Hermann-Rein-Str. 3, D-37075 Göttingen, Germany.

Email: sgoebbels@mpinat.mpg.de and nave@mpinat.mpg.de

Funding information

European Research Council; Deutsche Forschungsgemeinschaft, Grant/Award Number: SPP1757

Abstract

Oligodendrocytes and astrocytes are metabolically coupled to neuronal compartments. Pyruvate and lactate can shuttle between glial cells and axons via monocarboxylate transporters. However, lactate can only be synthesized or used in metabolic reactions with the help of lactate dehydrogenase (LDH), a tetramer of LDHA and LDHB subunits in varying compositions. Here we show that mice with a cell type-specific disruption of both *Ldha* and *Ldhb* genes in oligodendrocytes lack a pathological phenotype that would be indicative of oligodendroglial dysfunctions or lack of axonal metabolic support. Indeed, when combining immunohistochemical, electron microscopical, and in situ hybridization analyses in adult mice, we found that the vast majority of mature oligodendrocytes lack detectable expression of LDH. Even in neurodegenerative disease models and in mice under metabolic stress LDH was not increased. In contrast, at early development and in the remyelinating brain, LDHA was readily detectable in immature oligodendrocytes. Interestingly, by immunoelectron microscopy LDHA was particularly enriched at gap junctions formed between adjacent astrocytes and at junctions between astrocytes and oligodendrocytes. Our data suggest that oligodendrocytes metabolize lactate during development and remyelination. In contrast, for metabolic support of axons mature oligodendrocytes may export their own glycolysis products as pyruvate rather than lactate. Lacking LDH, these oligodendrocytes can also “funnel” lactate through their “myelinic” channels between gap junction-coupled astrocytes and axons without metabolizing it. We suggest a working model, in which the unequal cellular distribution of LDH in white matter tracts facilitates a rapid and efficient transport of glycolysis products among glial and axonal compartments.

This is an open access article under the terms of the [Creative Commons Attribution-NonCommercial-NoDerivs](https://creativecommons.org/licenses/by-nc-nd/4.0/) License, which permits use and distribution in any medium, provided the original work is properly cited, the use is non-commercial and no modifications or adaptations are made.

© 2024 The Authors. GLIA published by Wiley Periodicals LLC.

KEYWORDS

2',3'-cyclic nucleotide phosphodiesterase (CNP); glycolysis; lactate, lactate dehydrogenase (LDH, LDHA, LDHB); metabolic support; myelin; oligodendrocyte; optic nerve; white matter

1 | INTRODUCTION

A central role in brain energy metabolism is played by glial cells, which are metabolically coupled by gap junctions and monocarboxylate transporters to each other and to neuronal compartments. Several studies have suggested an important function of astroglia-derived lactate as an energy substrate of neuronal oxidative metabolism, based on the concept of the “astrocyte-to-neuron lactate shuttle” (ANLS) (Allaman et al., 2011; Brown et al., 2004; Obel et al., 2012; Pellerin & Magistretti, 1994, 2004, 2012). While the original ANLS has been controversially discussed (Albanese et al., 2016; Bosoi & Rose, 2014; Dienel, 2017; Liguori et al., 2015; Yellen, 2018), it has also gained considerable experimental support by in vitro (Bouzier-Sore et al., 2003; Karagiannis et al., 2021) and in vivo studies (Mächler et al., 2016; Suzuki et al., 2011; Wyss et al., 2011; Zuend et al., 2020).

The energy supply in white matter tracts constitutes a special problem because myelinated axons are physically deprived from the metabolites of the extracellular milieu by myelin itself (Nave, 2010). In search for a mechanism, we found that mature oligodendrocytes survive well in *Cox10* (protoheme IX farnesyltransferase)-deficient mice, in which oligodendrocytes lack an assembly factor of stable mitochondrial cytochrome c oxidase (COX, mitochondrial complex IV). This is compatible with the idea that adult oligodendrocytes become predominantly glycolytic with a reduced rate of oxidative phosphorylation (OXPHOS) (Fünfschilling et al., 2012). This led to a working model of glycolytic oligodendrocytes providing direct metabolic support to axons via non-compacted cytoplasmic channels in myelin and monocarboxylate transporters, which preserves functional integrity and axon survival (Amaral et al., 2013; Fünfschilling et al., 2012; Lee et al., 2012). The model is further supported by ex vivo electrophysiological recordings of compound action potentials in optic nerves under defined metabolic conditions and with the help of neuronally expressed ATP sensors (Saab et al., 2016; Trevisiol et al., 2017). It is finally in agreement with axonal degeneration observed in mice lacking the monocarboxylate transporter MCT1 in oligodendrocytes lineage cells (Lee et al., 2012; Philips et al., 2021). However, there is so far no experimental approach to the question of whether oligodendrocytes release lactate or pyruvate (Fünfschilling et al., 2012) for the support of axonal energy metabolism. A priori, pyruvate could serve the same metabolic functions as lactate in myelinated tracts, as long as oligodendrocytes can oxidize NADH and regenerate the NAD⁺ that is spent in glycolysis.

Lactate can only be generated from pyruvate by lactate dehydrogenases (LDH), necessitating a careful analysis of LDH expression in white matter tracts. In mammals, three *Ldh* genes give rise to subunits (LDHA, LDHB, LDHC) that form tetrameric LDH isoenzymes. While LDHA and LDHB are widely expressed including brain (Miura, 1966a; Miura, 1966b; Ross et al., 2010), LDHC is restricted to testis and

sperm (Goldberg et al., 2010). LDH catalyzes the bidirectional conversion of pyruvate and lactate, with LDHA reportedly having a higher affinity for pyruvate (Claps et al., 2022; Mishra & Banerjee, 2019) and LDHB a higher affinity for lactate (Kopperschlager & Kirchberger, 1996; Read et al., 2001).

Here, we show in mice that most mature oligodendrocytes in the adult brain appear devoid of LDH expression, which may explain why also the oligodendroglia-specific disruption of both *Ldha* and *Ldhb* genes has no detectable phenotypical consequences. Therefore, our findings indicate that lactate synthesized by adult oligodendrocytes is unlikely a supporting metabolite for axons, suggesting pyruvate as a possible alternative. Moreover, in the optic nerve we found LDHA enriched at astrocyte-astrocyte gap junctions and on the astroglial side of astrocyte-oligodendrocyte junctions. This suggests that astroglial lactate is preferentially produced at sites of transcellular transport, compatible with a model of astroglial lactate routed through oligodendrocytes to the axonal compartment (Philippot et al., 2021). The virtual lack of LDH from mature oligodendrocytes and myelin separates astroglial and axonal lactate metabolism, enabling efficient lactate funneling without loss in oligodendroglial metabolism.

2 | METHODS

2.1 | Mice

Heterozygous mice harboring the *Ldha*^{tm1a(EUCOMM)Wtsi} allele (EM: 03785; also termed *Ldha*^{lacZ/neo}) and frozen mouse sperms harboring the *Ldhb*^{tm1a(KOMP)Wtsi} allele (EM: 08936; also termed *Ldhb*^{lacZ/neo}) were obtained from the European Mouse Mutant Archive (EMMA, Neuberger/Munich, Germany). Sperms were used for in vitro fertilization and heterozygous mice were used for breeding, yielding mice harboring the *Ldha*^{lacZ/neo} or *Ldhb*^{lacZ/neo} alleles, respectively. Upon intercrossing each line with mice expressing FLIP recombinase (129S4/SvJaeSor-Gt(ROSA)26Sor^{tm1(FLP1)Dym}/J; backcrossed into C57BL/6N) the lacZ/neo cassette was excised in vivo, yielding the “conditional ready” flox alleles in mice carrying the *Ldha*^{tm1c(EUCOMM)Wtsi} or *Ldhb*^{tm1c(KOMP)Wtsi} allele (also termed *Ldha*^{flox} and *Ldhb*^{flox}), respectively. To inactivate expression of *Ldha* and *Ldhb* simultaneously in oligodendrocytes, exon 3 was excised from each gene in vivo upon the generation of phenotypically normal *Ldha*^{flox/flox}; *Ldhb*^{flox/flox}; *Cnp*^{Cre/+} mice that additionally expressed *Cre* under the control of the *Cnp* promoter (*Cnp*^{tm1(crc)Kan}) (Lappe-Siefke et al., 2003). For simplicity, *Ldha*^{flox/flox}; *Ldhb*^{flox/flox}; *Cnp*^{Cre/+} mutant mice are also termed LDH-dKO or conditional double mutants (dKO). *Ldha*^{flox/flox}; *Ldhb*^{flox/flox}; *Cnp*^{+/+} harboring no *Cre* allele are termed controls (ctrl). To inactivate the expression of LDHA and LDHB specifically in mature oligodendrocytes, *Ldha*^{flox/flox}; *Ldhb*^{flox/flox} mice were intercrossed with mice expressing tamoxifen-

inducible Cre recombinase under the control of the *Plp* promoter (*PlpCreERT2* mice; Tg(*Plp1-cre/ERT2*)1Ueli) (Leone et al., 2003). Both *Ldha*^{flox/flox}; *Ldhb*^{flox/flox} mice (termed controls) and induced conditional knockout mice (*Ldha*^{flox/flox}; *Ldhb*^{flox/flox}; *PlpCreERT2*; termed LDH-idKO) were injected with tamoxifen intraperitoneally (i.p.) at the age of 8 weeks (1 mg tamoxifen dissolved in 100 µL corn oil per mouse per day) for 10 days with a break of 2 days after the first 5 days of injection. Routine genotyping for the detection of the *Ldha*⁺ and *Ldha*^{flox} alleles in mice was performed by genomic PCR on-ear clip DNA by using antisense primer P4 (5'-AGACAGGTACTTCGTC-CATGC-3') together with sense primers P1 (5'-CAGGCC-CAAGTCTCACTG-3'), P2 (5'-AGAGATGGCGCAACGCAATTAAT-3') and P3 (5'-CTTATGGGTTCTGGAGATGAAATTCAGC-3'), amplifying a 292 bp product from the wt allele, a 353bp product from flox allele and a 537 bp product from the recombined flox allele. *Ldhb*⁺ and *Ldhb*^{flox} alleles were detected by using sense primer P5 (5'-GTAGATGATTGAATACCATACTCC-3') in combination with antisense primers P6 (5'-AGTCTGCTACTGTGCTGTC-3') and P7 (5'-GACCTTCTGGAGTGCTG-3') amplifying a 224 bp product from the wt allele, a 415 bp product from the flox allele and a 537 bp product from the recombined flox allele. PCR genotyping of *PlpCreERT2* was performed with primers 5'-TGGACAGCTGGACAAAGTAAGC-3' and 5'-CGTTGCATCG ACCGGTAATGCAGGC-3', amplifying a 250 bp band in heterozygous *PlpCreERT2* mutant mice. *Cnp*^{Cre} and *Cnp*^{wt} alleles were identified by genomic PCR with primers 5'-GCCTTCAAAGTGC-CATCTC-3', 5'-CCCAGCCCTTTATTACCAC-3', and 5'-CATAGCCT-GAAGAACCAGA-3' amplifying a 700 kb product from the wt allele and a 400 bp product from the Cre allele. Conditional *Cox10*^{flox/flox}; *Cnp*^{Cre/+} mice (*Cox10*^{tm1Ctm}) (Fünfschilling et al., 2012), *Plp*^{null} mice (*Plp1*^{tm1Kan}) (Klugmann et al., 1997), 5x*FAD* mice (Tg(*APPSwFILon*,*PSEN1**M146L*L286V)6799Vas) (Oakley et al., 2006), and *App*^{NLGF} mice (*App*^{tm3.1Tcs}) (Saito et al., 2014) were genotyped as described in the referenced publications. Experimental mutant mice were analyzed together with littermate controls as far as possible. Both male and female mice were used throughout the study. Mice were housed with ad libitum access to water and food in standard plastic cages with 1–5 littermates in a temperature-controlled room (~21°C) under a 12 h/12 h light/dark cycle in the mouse facility of the Max Planck Institute for Multidisciplinary Sciences (MPI-NAT). Animal experiments were performed in accordance with the German animal protection law (TierSchG) and approved by the Niedersächsisches Landesamt für Verbraucherschutz und Lebensmittelsicherheit (LAVES) under licenses 33.19-42,502-04-17/2437, 33.19-42,502-04-17/2400, 3392 42,502-04-13/1168, 33.8-42,502-04-19/3116, and 509.42502/02-03.00.

2.2 | Expression analyses

For the characterization of *Ldha* and *Ldhb* gene expression, mice were killed by cervical dislocation, and pooled white matter enriched samples (Corpus callosum) were quickly prepared on ice. RNA was extracted using QIAzol (Quiagen) and RNeasy Mini kit (Qiagen). The purity and concentration of RNA was evaluated using a NanoDrop

TABLE 1 List of primer sequences.

Gene	Sequence (5'-3'; forward–reverse)
<i>Ldha</i>	TGGCAGCCTTCTCTTAAAA- CAGCTTGGAGTTCGCAGTTA
<i>Ldhb</i>	CCTCCAGACTCCGAAAATTG- TCTCTGCACCAGGTTGAGC
<i>Rplp0</i>	GATGCCAGGGAAGACAG- ACAATGAAGCATTGATAATCA
<i>Rps13</i>	CGAAAGCACCTTGAGAGAA- TTCCAATTAGGTGGGAGCAC

spectrophotometer and RNA Nano (Agilent). cDNA was synthesized by using Superscript III (Invitrogen, Carlsbad, CA, USA) according to the manufacturers' instructions. Quantitative RT-PCR (qRT-PCR) was performed in quadruplicates with the GoTaq qPCR Master Mix (Promega) on a LightCycler 480 Instrument (Roche Diagnostics). Expression values were normalized to the mean of the house keeper genes *Rps13* (Ribosomal protein S13) and *Rplp0* (Ribosomal Protein Lateral Stalk Subunit P0). Relative expression changes were analyzed using the $2^{-\Delta\Delta C(T)}$ method, normalized to experimental controls (set to 1). All primers (Table 1) were designed with Universal Probe Library from Roche Applied Systems (<https://www.roche-applied-science.com>) and validated with NIH PrimerBlast. All primers were intron-spanning.

2.3 | Immunoblotting

Microdissected Corpus callosum samples were homogenized in 200 µL ice-cold modified RIPA buffer (1× TBS, 1 mM EDTA, 0.5% [wt/vol] sodiumdeoxycholate, 1.0% [vol/vol] Triton X-100, cOmplete™ Mini protease inhibitor (Roche Diagnostics) using ceramic beads and a Precellys 24 Tissue Homogenizer (Bertin Instruments, France) at a homogenization speed of 5000 rpm for 10s (4°C). The homogenates were centrifuged for 10 min at 13000 rpm (4°C) to remove undissolved tissue. The protein concentration of the supernatant was determined in triplicates using the detergent-compatible Biorad DC protein assay. Subsequently, samples were mixed with sample buffer to a final concentration of 2% (wt/vol) LDS, 0.125% (vol/vol) Triton X-100, 0.125% (wt/vol) sodium deoxycholate, 0.501 mM EDTA, 10% glycerol, 247 mM Tris-HCl [pH 8,4], 0.01875% (wt/vol) Coomassie G250, 0.00625% (wt/vol) phenol red, 25 mM DTT and 1 µg/µL total protein and heated at 40°C for 10 min. 15 µL lysate corresponding to 15 µg total protein was loaded per lane and separated on 12% polyacrylamide-SDS gels in Laemmli sample buffer for 1.5 h at 120 V using the Mini protean chamber (Biorad). Proteins were transferred onto a PVDF Membrane (Immobilon-FL PVDF, IPFL00010, Merck Millipore) in transfer buffer (25 mM Tris, 192 mM Glycine, 10% Methanol) using a XCell II™ Blot Module (ThermoFisher) for 1 h at 38 V. To verify equal loading, blots were stained by fast green (5 mg/L fast green, Sigma, in 6.7% [vol/vol] acetic acid and 30% [vol/vol] methanol) immediately after transfer for

5 min, washed twice for 30s in 6.7% (vol/vol) acetic acid and 30% (vol/vol) methanol, and imaged using a near-infrared fluorescence scanner (Odyssey, Licor). Total protein per lane was quantified using the Image Studio Software (Licor). Blots were destained in 50% (vol/vol) ethanol in TBS (150 mM NaCl, 10 mM Tris/HCl [pH 7.4]), blocked with 5% (wt/vol) skim milk in TBS for 1 h and subsequently incubated with primary antibodies directed against LDHA, LDHB or actin (see Table 2) on a rotating shaker. Antibodies were diluted in 5% (wt/vol) skim milk in TBST (150 mM NaCl, 10 mM Tris/HCl [pH 7.4], 0.5% [vol/vol] Tween 20), and incubated for 48 h at 4°C. After washing with TBST, blots were incubated with near-infrared fluorophore-coupled secondary antibodies diluted in 5% (wt/vol) skim milk in TBST (1:10,000, Mouse IgG [H&L] Antibody DyLight 680 Conjugated, 610-144-002; Rabbit IgG [H&L] Antibody DyLight 800 Conjugated, 611-145-002; Rockland), washed with TBST, and detected using the Odyssey platform (Licor). For quantification of protein abundance, images obtained from the near-infrared fluorescence imager were analyzed using the Image Studio software (Licor). Signal intensities for LDHA and LDHB were normalized to the intensity of the corresponding actin signal in the same lane. Normalized signal intensities for LDHA and LDHB were further normalized to the mean of the respective signal intensity from control mice (set to 1).

2.4 | Primary oligodendrocyte cultures and immunocytochemistry

Primary oligodendrocyte cultures were essentially prepared as described (Weil, Schulz-Éberlin, et al., 2019b). Briefly, P8-P9 mouse brains (wild type, C57Bl/6-N) were dissected and dissociated under sterile conditions using the Neural Tissue Dissociation Kit (Milteny Biotec) and the gentleMACS™ Octo Dissociator (Milteny Biotec). Following tissue dissociation OPCs were isolated by magnetic activated cell sorting (MACS) using anti-NG2-coupled MicroBeads (Milteny Biotec). OPCs were plated at a density of 12×10^4 cells per 12 well plate and cultured in proliferation medium (100 mL NeuroMACS media, 2 mL MACS NeuroBrew21, 1 mL Pen/Strep, 1 mL L-GlutaMAX, 100 μ L Forskolin, 100 μ L CNTF, 100 μ L PDGF, 100 μ L NT-3), which was replaced with OPC differentiation medium (100 mL NeuroMACS media, 2 mL MACS NeuroBrew21, 1 mL Pen/Strep, 1 mL L-GlutaMAX, 100 μ L Forskolin, 100 μ L CNTF, 100 μ L T3) at DIV4. At DIV6 oligodendrocytes were fixed in 4% PFA (10 min) and permeabilized in 0.3% Triton X-100 in PBS (RT, 15 min). Following washing steps in PBS (5 min), and blocking in 10% normal goat serum (NGS) + 0.3% Triton X-100 in PBS (1 h) cells were incubated in primary antibodies directed against LDHA or LDHB together with antibodies against MBP (see Table 2) over night at 4°C in blocking solution. Cells were washed 3 \times in PBS and incubated in secondary antibodies for 1 h (Alexa488 donkey anti-mouse, Invitrogen, 1:1000; Alexa555 donkey anti-rabbit, Invitrogen, 1:1000) with DAPI (0.5 μ g/mL), washed 3 \times in PBS and mounted using Aqua Poly/Mount (Polysciences, Germany).

2.5 | X-gal histochemistry

Mice were anesthetized with a lethal dose of avertin and perfused through the left ventricle with 4% paraformaldehyde (PFA) in 0.1 M phosphate buffer. Brains were dissected and postfixed overnight in 4% paraformaldehyde (PFA). For X-gal histochemistry brains were sectioned in phosphate-buffered saline (PBS) on a vibratome (Leica VT 1000S, Leica Instruments, Nussloch, Germany) and free-floating sections (30–200 μ m) were incubated at 37°C in X-gal solution (5 mM K₃[Fe(CN)₆], 5 mM K₄[Fe(CN)₆], 2 mM MgCl₂, 1.2 mg/mL 5-bromo-2-chloro-3-indoyl-b-D-galactopyranoside (X-gal) in PBS) for up to 16 h in the dark, rinsed in water, and mounted in Kaiser's gelatin (Merck) or further utilized for fluorescent immunohistochemistry as described (Hirrlinger et al., 2006) by using primary antibodies directed S100b or Olig2 (see Table 2) and Cy2- or Cy3-conjugated secondary antibodies (1:1000, Dianova).

2.6 | Immunohistochemistry

Mice were anesthetized with a lethal dose of avertin and perfused through the left ventricle with Hanks balanced salt solution followed with 4% paraformaldehyde (PFA) in 0.1 M phosphate buffer. Brains were dissected, post-fixed overnight in 4% PFA, paraffinized using a Microm STP 120 Spin Tissue Processor (Thermo Scientific) and then embedded in paraffin blocks on a HistoStar embedding workstation (EpreDia). 5 μ m brain sections were performed on a RM2155 (Leica) rotary microtome and were mounted on adhesive microscope slides (Histobond). Slices were deparaffinized at 60°C and rehydrated using xylene and a descending ethanol series. Heat-induced epitope-retrieval was performed in sodium citrate buffer (0.01 M, pH 6.0, 10 min in a 400-Watt microwave with a 20 min cooldown period). For immunohistochemical antibody detection through chromogenic reaction endogenous peroxidase activity was blocked with 3% hydrogen peroxide. Subsequently, slides were blocked for 1 h at RT in 20% goat serum (BSA/PBS) and incubated with primary antibodies (anti-MAC3, anti-GFAP, anti-APP, anti-CD3, see Table 2) at 4°C overnight. Detections were carried out with the LSAB2 system-HRP kit (DAKO) or the VECTASTAIN Elite ABC HRP kit (Vector labs). The HRP substrate 3,3'-Diaminobenzidine (DAB) was applied by utilizing the DAB Zytomed kit (Zytomed Systems GmbH). Nuclei were labeled by Hematoxylin stain. Sections were imaged with a bright-field light microscope (Zeiss Axio Imager Z1 equipped with a Zeiss AxioCam MRc camera) and ZEN 2012 blue edition software. Images of hippocampal fimbriae were color deconvoluted using the "Color Deconvolution" (1.3) plugin in Fiji/ImageJ. GFAP⁺ and MAC3⁺ areas were quantified using thresholding, and CD3 cells and APP spheroids were quantified manually using the "Cell counter" plugin from Fiji/ImageJ. All data were normalized to the respective quantified areas. For immunohistochemical antibody detection through fluorescent reaction non-specific epitopes were blocked by incubating in 5% normal goat serum (NGS) and 2% bovine serum albumin

TABLE 2 Primary Antibodies.

Antibody	Source/company	Catalog/lot/clone	WB	Immuno EM	IC/IHC
rb anti-LDHA	PTAG	19,987-1-AP	1:1000	-	-
rb anti-LDHA	Novus	NBP1-48336/B5	-	1:100	1:200
rb anti-LDHA	Invitrogen	PA5-17183/	-	-	1:50
rb anti-LDHB	Novus	NBP1-55415	1:1000	1:100	1:200
m anti-NeuN	Chemicon	MAB377	-	-	1:100
rat anti-CAII	S. Ghandour	CAII, AB_2314062	-	1:200	1:200
m anti-APC (CC1)	Oncogene	OP80	-	-	1:50
m anti-MBP	Novocastra	NCL-MBP/7H11	-	-	1:100
rat anti-Iba1	Abcam	ab5076	-	-	1:2000
m anti-GFAP	Chemicon	MAB-3402	-	-	1:200
rat anti-MAC3	Pharmingen	553322	-	-	1:500
rat anti-CD3	Abcam	ab11089	-	-	1:250
rb anti-S100b	Abcam	ab52642	-	-	1:200
m anti-APP	Millipore	MAB348/3200582	-	-	1:1000
m anti-A β	Biologend	6E10	-	-	1:1000
m anti-Actin	Sigma	A3853	1:10000	-	-
rb anti-MCT1/SLC16a1	(Stumpf et al., 2019)	-	-	1:50	-
rb anti-SIRT2	Proteintech	15345-1-AP	-	1:300	-
rb anti-Olig2	Charles D. Stiles	DF308, AB_2336877	-	-	1:200

(BSA) in PBS for 30 min. Next, sections were incubated overnight with primary antibodies diluted in 2% BSA/PBS. Utilized primary antibodies were directed against NeuN, CC1, LDHA, LDHB, PLP, A β , GFAP and CAII (see Table 2). After washing with PBS, sections were incubated with fluorophore-coupled secondary antibodies (Alexa555 donkey anti-rabbit, Invitrogen, 1:1000; Alexa555 donkey anti-mouse, Invitrogen, 1:1000; DL633 goat anti-rabbit, Invitrogen 1:500; DL633 goat anti-mouse, Invitrogen 1:500; Cy5 goat anti-rat, Dianova 1:500), all diluted in 10% goat serum in PBS. Slides were mounted with Aqua Poly/Mount and imaged using an Axio Imager. Z1 (Zeiss) equipped with a Colibri 7 solid state light source using an ORCA-Fusion CMOS Camera (C14440-20UP, Hamamatsu). Image analysis was conducted with ZEN 2012 blue edition software and using ImageJ/Fiji software. For the quantification of colocalization of LDHA and LDHB with NeuN⁺ neurons and CAII⁺ or CC1⁺ oligodendrocytes images of brain sections were analyzed from adult control mice ($n = 3$, except for brain stem, $n = 2$; age: 6 months), developing control mice ($n = 3-4$ per age; ages: P10, P15, P25, P75), and cuprizone-treated mice ($n = 3$; age: 8-10 weeks +6 weeks on cuprizone treatment). Background reduction was done by subtracting a 100 px median filtered image. Cells were quantified via thresholding and the ImageJ function “Analyze Particles” as well as manually with the “Cell counter” plugin. LDHA fluorescence intensity was quantified in 20 randomly chosen LDHA⁺; CC1⁺ oligodendrocytes per age and condition while subtracting local background values (estimated as before), and normalized to P10. All analyses were performed blind to the conditions of the mice.

2.7 | Gallyas silver impregnation

For Gallyas silver impregnation (Gallyas, 1979; Joseph et al., 2019) paraffin sections were deparaffinized and non-myelin tissue staining was suppressed through a 30 min incubation in a fresh pyridine/acetic anhydride mixture (2:1), followed by three 5 min washes in ddH₂O. The sections were submerged in ammonium nitrate, silver nitrate (pH 7.4) and microwaved at 440 W for 2 min at ~50°C, cooled down for 10 min at room temperature, then washed in 5% acetic acid. Sections were developed in sodium carbonate anhydrous, ammonium nitrate, silver nitrate, tungstosilicic acid hydrate, formaldehyde for 3-15 min. The reaction was stopped with 1% acetic acid. Staining was fixed through a 5 min incubation in 2% sodium thiosulfate. Dehydration was carried out through sequential 5 min immersions in 50%, 70%, 90%, 100% ethanol, 2-propanol/xylene (1:1), and two 10 min immersions in xylene. Sections were mounted in Aqua Poly/Mount.

2.8 | Electron microscopy

For conventional transmission electron microscopy (TEM) optic nerves were dissected, immersion-fixed in fixative (4% PFA, 2.5% glutaraldehyde in 0.1 M phosphate buffer) at 4°C and embedded in epoxy resin (Serva) as described (Weil, Ruhwedel, et al., 2019a). Ultrathin sections (50 nm) were cut using a PTPC Powertome Ultramicrotome (RMC, Tuscon Arizona, USA) and collected on formvar polyvinyl-coated double-sized slot grids (AGAR scientific, Essex, UK). Ultrathin sections were contrasted with UranylLess (Electron Microscopy Science,

Hatfield, Panama) for 15–30 min and washed six times with d_4H_2O . Sections were viewed using a LEO EM912AB-Omega (Zeiss, Oberkochen, Germany) coupled to an on-axis 2048 × 2048-CCD camera (TRS, Moorenweis, Germany) at ×9600 magnification.

2.9 | Immuno electron microscopy

Immunogold labeling of cryosections prepared according to the Tokuyasu method was performed as described by the experimenter blinded to the genotype of the animals (Peters & Pierson, 2008; Weil, Ruhwedel, et al., 2019a). Optic nerves were dissected and immersion-fixed in fixative (4% PFA, 2.5% glutaraldehyde in 0.1 M phosphate buffer) overnight, infiltrated with 2.3 M sucrose in 0.1 M phosphate buffer, mounted onto aluminum pins, and flash-frozen in liquid nitrogen. Ultrathin cryosections (50–80 nm) were cut with a diamond knife (Diatome, Biel, Switzerland) using a Leica UC6 cryo-ultramicrotome. Primary antibodies used were directed against LDHA, LDHB, CAII, MCT1, and SIRT2 (see Table 2). Colloidal gold conjugated to protein A was obtained from the Cell Microscopy Center (Department of Cell Biology, University Medical Center at Utrecht, The Netherlands) and prepared as done previously (Roth et al., 1978; Slot & Geuze, 1985). Samples were analyzed using a LEO EM912AB-Omega (Zeiss, Oberkochen, Germany) coupled to an on-axis 2048 × 2048-CCD camera (TRS, Moorenweis, Germany). G-ratio analysis and quantifications of gold particles in axons, myelin sheaths, astrocytes, and oligodendrocytes were performed on 12–13 individual immunoelectron micrographs of optic nerves with an area of 16.86 μm^2 each from 11-month-old mice (4 per genotype) at a magnification of ×9.600. G-ratios were determined by dividing axon diameter by the diameter of the entire fiber. Axon density was measured by counting the number of axons and dividing it by the area. For LDHA quantification, individual gold particles were counted manually in axons, myelin, astrocytes, and oligodendrocytes and then normalized to their respective areas. Because of sparse labeling, LDHB quantification was performed similarly with the exception that the number of gold particles within all myelin sheaths and axons in individual electron micrographs was summed up and normalized to the number of myelinated axons in each image. To compare effects of the dKO on LDHA and LDHB expression in oligodendrocyte somata and myelin, we further normalized the expression to the control. Quantifications were performed with ImageJ/Fiji and the experimenter blinded to the genotype.

2.10 | In situ hybridization

For in situ RNA expression analysis we employed the RNAscope® Multiplex Fluorescent Reagent kit v2 Assay (Advanced Cell Diagnostics, Inc.) using the standard protocol for formalin-fixed, paraffin-embedded sections (see RNAscope® Sample Preparation and Pretreatment Guide for FFPE Tissue, #320511 and RNAscope® Fluorescent Multiplex Kit User Manual, #320293). Incubation was done using a humid control tray (PN 310012) and HybEZ Humidifying

Paper (PN 310025), for 40/60°C incubation the HybEZ oven (PN 321710/321720) was used. Briefly, we first baked slices at 60°C for 1 h. Sections were then deparaffinized using xylene and ethanol. Samples were pretreated with RNAscope® hydrogen peroxide (15 min, RT). Target retrieval was performed with RNAscope® Target Retrieval buffer (30 min, 40°C) and RNAscope® Protease Plus (30 min, 40°C). Hybridization was performed for 2 h at 40°C. Hybridization probes were Mm-Ldhb (545101) and Mm-Ldha-C2 (313711-C2). Amplification of C1 was done using RNAscope® Multiplex FL v2 Amp1, Amp2, and Amp3 for 30 min each at 40°C. For development, we incubated with Multiplex FL v2 HRP-C1 (15 min, 40°C) and Opal™ 570 (30 min, 40°C). Amplification of C2 was done the same but using Opal™ 690. Finally, slices were counterstained with DAPI and mounted with Aqua-Poly/Mount. In between steps slides were washed in TBS. For quantitative analysis, individual cell nuclei in the Corpus callosum were marked and the number of RNA dots associated with each nucleus were counted, including dots directly adjacent to the nucleus. A total of 5522 individual cells were quantified distributed over six animals.

2.11 | Cuprizone

Wildtype mice (age 8–10 weeks) were fed with powdered chow supplemented with 0.2% wt/wt cuprizone ad libitum (Sigma-Aldrich Inc., Germany) for a total of 5 weeks (peak of demyelination) or 6 weeks (peak of spontaneous remyelination), as described (Berghoff et al., 2017).

2.12 | Reanalysis of single-cell RNA sequencing data from mouse CNS

Publicly available single-cell resolution RNA-seq datasets were acquired from the Gene Expression Omnibus (GEO) repository. Specifically, expression metrics and meta data from GSE129788 (Ximerakis et al., 2019) and GSE140511 (Zhou et al., 2020) were collected and processed for reanalysis using R package Seurat V4.0.0 (Hao et al., 2021). Analysis procedure and parameters were identical to the original publications, with cell type annotations cross-checked using calculated cluster marker genes. For further analysis, major cell populations including oligodendrocyte precursor cells (OPC), committed oligodendrocytes precursor cells (COP), mature oligodendrocytes (OI), neurons (N), astrocytes (As), microglia (Mi), and endothelial cells (EC) were subset, and only cells from wild type animals were included. Subsequently, expression of glycolytic genes was visualized with DotPlot function implemented in the Seurat package. For each gene, positive expression rates were calculated and visualized by barplot using R package ggplot2 (3.4.2).

2.13 | Software

Statistical analysis and graphs were done using GraphPad Prism (9.4.0) and R (4.1.3). Image acquisition and stitching were done using

ZEN 2012 blue edition (widefield microscopy) and Olympus (scanning confocal microscopy). Image analysis was performed in Fiji/ImageJ (2.9.0/1.53t).

2.14 | Statistics

All data acquisition was performed blinded. Bar graphs represent means, and errors are reported as the standard error of the mean (SEM). Student's *t* test and ANOVAs were conducted in GraphPad. For multiple comparisons, we used either Tukey or Šidák. In instances where multiple data points per animal (i.e., replicates) were collected (g-Ratio analyses, RNAscope quantification, immuno electron microscopy analyses) a (generalized) linear mixed model ((G)LMM) was fitted via restricted maximum likelihood (REML) method using the lme4 package (1.1.33) in R. All models were intensively checked using the DHARMA (0.4.6) and performance (0.10.4) R packages to verify assumptions and fit. Estimated marginal means and pairwise comparisons were calculated using the emmeans package (1.8.7), which uses Kenward-Rodger method for degrees of freedom, and Tukey method to adjust *p*-values when testing multiple comparisons. *p*-values less than .05 were considered statistically significant. Statistical power of the LMMs was estimated using a simulation-based power analysis ($n = 1000$). The fully annotated R script including all verifications of the models and power analysis is available on GitHub (<https://github.com/espate/LDHAB-Oligodendrocytes>).

3 | RESULTS

3.1 | Conditional inactivation of *Ldha* and *Ldhb* in oligodendrocytes

To better understand the role of myelinating glia in CNS lactate metabolism, we generated floxed *Ldha* and floxed *Ldhb* mutant mouse lines for the conditional inactivation of these genes in oligodendrocytes (Figure 1a). Since LDHA and LDHB can compensate for each other (Urbańska & Orzechowski, 2019), only the inactivation of both genes ensures that lactate is neither generated nor utilized in metabolic reactions. We first used a tamoxifen-inducible transgenic *PlpCreERT2* driver line (Leone et al., 2003) for temporally controlled inactivation of both genes in oligodendrocytes of young adult *Ldha^{flox/flox}; Ldhb^{flox/flox}; PlpCreERT2* mice (hereafter termed idKO). IdKO mice and their respective controls lacking Cre (*Ldha^{flox/flox}; Ldhb^{flox/flox}*; hereafter termed ctrl) were injected intraperitoneally with tamoxifen at the age of 8 weeks and analyzed at age 18 weeks (Figure 1a). IdKO mice were indistinguishable by appearance and cage behavior from control mice up to the latest assessed age (6 months).

To study possible pathological consequences, we performed histological analyses of adult mutants, which appeared properly myelinated in the CNS by Gallyas silver impregnation (Figure 1b). Immunohistological analysis of glial fibrillary acidic protein (GFAP) revealed a normal astroglial scaffold and no signs of astrogliosis (Figure 1b,c).

Stainings for MAC3 as a marker for activated microglia, CD3 as a marker for infiltrating T-cells, and amyloid precursor protein (APP) as a surrogate marker for axonal transport defects indicated the absence of inflammation and axonal swellings (Figure 1b,c). We confirmed Cre-mediated recombination of both genes at genomic level by PCR using isolated Corpus callosum tissue lysates (Figure 1d). Surprisingly, both western blot and qRT-PCR analyses isolated from the same Corpus callosum material did not reveal significant quantitative differences of *Ldha* and *Ldhb* mRNA and LDH protein when comparing idKO and controls (Figure 1d). Thus, either other cells had upregulated LDHA and LDHB expression as a consequence of oligodendroglial ablation, or *PlpCreERT2* had recombined the floxed genes to an insufficient degree, or oligodendrocytes contributed only marginally to *Ldh* mRNA and protein in the adult Corpus callosum.

To address these possibilities, we ensured the complete inactivation of the floxed *Ldh* genes in oligodendrocytes by using the *Cnp^{Cre}* driver line (Lappe-Siefke et al., 2003) that recombines floxed genes to virtually 100% in oligodendrocytes and up to 60% of OPCs (Madsen et al., 2016; Saab et al., 2016; Vajda et al., 2015). However, *Cnp^{Cre}* mice also recombine Schwann cells and off-target in subsets of CNS neurons including motoneuronal precursors (Genoud et al., 2002; Jo et al., 2021; Tognatta et al., 2017) (Figure S1a–e). The deletion of *Ldh* genes in Schwann cells and motoneurons causes a marked neuropathology (Bloom et al., 2022). Thus, we refrained from the histopathological analysis of brain and spinal cord of *Ldha^{flox/flox}; Ldhb^{flox/flox}; Cnp^{Cre}* double mutant mice (hereafter referred to as dKO, Figure 1a). Instead, we turned to the analysis of the optic nerve, a well-myelinated white matter tract, in which all *Cnp^{Cre}* recombined cells are of oligodendroglial origin (Saab et al., 2016).

By transmission electron microscopy (EM) at the age of 7 months, dKO nerves lacked signs of axonal pathology or degeneration (Figure 1e). Moreover, g-ratio analysis demonstrated a normal myelin thickness when compared to controls ($p = .1324$) (Figure 1e). Thus, although oligodendrocytes use lactate as an energy source in vitro (Sánchez-Abarca et al., 2001), in the presence of other nutrients normal myelin thickness in reached in vivo without utilization of lactate.

Next, we sought to determine the cellular identity of LDHA and LDHB-expressing cells in the optic nerve by quantitative immunogold EM labeling using specific antibodies against LDHA and LDHB, respectively. Mature oligodendrocytes were defined by morphology and by co-immunolabeling of carbonic anhydrase II (CAII; visualized by 15 nm gold particles; Figure 1f) and thus clearly distinguishable from astrocytes that were identified by their characteristic intermediate filaments and nuclear morphology. When quantifying immunogold-labeled LDHA and LDHB in control mice at age 11 months, we found the enzyme at a much higher level in astrocytes and axons than in myelin and oligodendroglial cell bodies (Figure 1f). Importantly, the low number of LDH-immunogold particles detected in oligodendrocytes and myelin of control mice was not further reduced in dKOs and thus presumably reflecting background level of immunolabeling (Figure 1g).

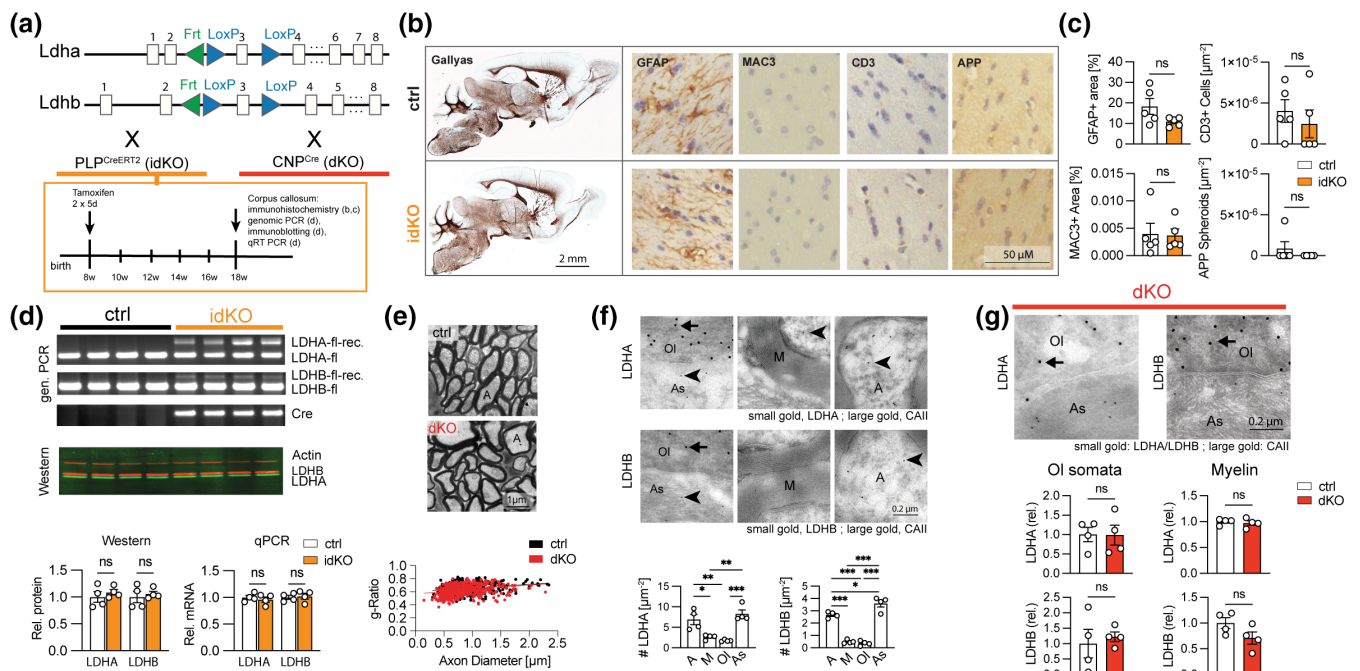


FIGURE 1 Simultaneous inactivation of LDHA and LDHB in oligodendrocytes by *PlpCreERT2* and *Cnp^{Cre}* driver lines. (a) Top: schematic depiction of *Ldha* and *Ldhb* gene structures with exon 3 of either gene flanked by loxP sites and excised by *PlpCreERT2* and *Cnp^{Cre}* driver lines. Bottom: schematic overview of the experimental design and time points of tamoxifen (TM) injection and analysis of idKO mice as shown in b–e. (b) Representative brain sections stained by Gallyas silver impregnation and magnifications of hippocampal fimbriae of idKOs and controls immunostained for GFAP, MAC3, CD3, and APP. (c) Quantitative assessments of immunostainings in b for relative GFAP⁺ area, relative MAC3⁺ area, CD3⁺ cell density, and APP⁺ spheroid density show absence of neuroinflammation and axonal pathology in idKOs ($p_{\text{GFAP}^+} = 0.101$, $p_{\text{MAC3}^+} = 0.906$, $p_{\text{CD3}^+} = 0.492$, $p_{\text{APP}^+} = 0.347$; unpaired, two-tailed Student's *t* test; age, 11 weeks; $n = 5$ per genotype). (d) Molecular analysis of *PlpCreERT2* driven recombination in white matter enriched tissue (Corpus callosum). Upper panel: Genomic PCR validates TM-induced Cre-mediated recombination for both genes in idKOs versus controls (ctrl) ($n = 4$ per genotype). Middle panel: Representative immunoblot using two-color infrared fluorescent protein detection of LDHA and LDHB (re-probed for actin signals) indicates similar levels of protein expression in controls and idKOs. Lower panels: Quantification of immunoblot ($n = 4$ per genotype; normalized to actin; $p_{\text{LDHA}} = 0.4608$, $p_{\text{LDHB}} = 0.6268$; unpaired, two-tailed Student's *t*-test; mean of controls set to 1) and quantification of relative mRNA expression by qRT-PCR analysis ($n = 4$ per genotype; $p_{\text{LDHA}} = 0.5581$, $p_{\text{LDHB}} = 0.7346$; unpaired, two-tailed Student's *t*-test; mean of controls set to 1) reveal unaltered protein and mRNA expression of LDHA and LDHB in the Corpus callosum of mutants when compared to controls. (e) Upper panel: Representative electron micrographs of optic nerves of 7 month-old dKO and ctrl. Lower panel: Scatter plot depicting *g*-ratios (ordinate) of mutants (red circles) and controls (black circles) in relation to axon diameters (abscissa) based on immuno electron micrographs from ultrathin cross sections of optic nerves at comparable levels at the age of 10 months. *G*-ratios of mutants are not significantly different from controls (total observations = 1030; $n = 4$ animals per genotype; $F(1, 8.28) = 2.79$; $p = .1324$; linear mixed model). (f) Immunogold labeling (top panels) and quantitative analysis (bottom panels) in optic nerves of control mice (age, 11 months) identifies LDHA and LDHB (10 nm gold particles, arrowheads) to be preferentially localized to axons and astrocytes but not to myelin and oligodendroglial somata (identified by CAII immunoreactivity in top panels, 15 nm gold particles, arrows) (LDHA: total observations = 172, $F(3, 8.93) = 19.74$, $p < .001$, $p_{\text{M-A}} = 0.009$, $p_{\text{M-As}} = 0.002$, $p_{\text{OI-As}} < 0.001$, $p_{\text{OI-A}} = 0.003$, $p_{\text{M-OI}} = 0.919$, $p_{\text{A-As}} = 0.518$; LDHB: total observations = 206, $n = 4$ animals per genotype, $F(3, 9.26) = 41.66$, $p < .001$, $p_{\text{M-A}} = 0.009$, $p_{\text{M-As}} < 0.001$, $p_{\text{OI-As}} < 0.001$, $p_{\text{OI-A}} < 0.001$, $p_{\text{M-OI}} = 0.977$, $p_{\text{A-As}} = 0.0103$, linear mixed model, $n = 4$ animals per genotype). (g) When compared to controls (representative images shown in f), dKO optic nerves at the age of 11 months (top panels) depict a similarly low immunogold-labeling for LDHA and LDHB (10 nm gold particles) in oligodendrocyte somata (identified by co-labeling for CAII, 15 nm gold particles; arrows). For quantitative analysis of immunogold-labeling in oligodendrocyte somata and myelin, linear mixed models were fitted to investigate effect of genotype on staining per μm^2 normalized to the controls (LDHA_{OI-somata}: total observations = 33, $p = .761$; LDHB_{OI-somata}: total observations = 36, $p = .654$; LDHA_{Myelin}: total observations = 103, $p = .191$; LDHB_{Myelin}: total observations = 111, $p = .118$, $n = 4$ animals per genotype). LMMs were fitted by REML. Post-hoc comparisons were conducted using the Tukey method to control for multiple testing. Kenward-Roger was used for degrees-of-freedom. Asterisks represent significant differences with * $p < .05$; ** $p < .01$; *** $p < .001$; ns not significant. A, axon; As, astrocyte; M, myelin; OI, oligodendrocyte.

3.2 | Oligodendrocytes are low in LDH by immunohistochemistry, in situ hybridization, and single-cell sequencing

Since the comparative analysis of conditional *Ldh* mutants and their respective controls unexpectedly failed to detect LDHA and LDHB in

adult wildtype oligodendrocytes, we conducted a more comprehensive expression analysis with complementary techniques.

By immunohistochemistry of different brain regions from adult control mice (age 6 months) we found both LDHA and LDHB foremost in neurons and also region-dependently in subsets of astrocytes (Figures 2, S2), but only rarely in oligodendrocytes throughout the

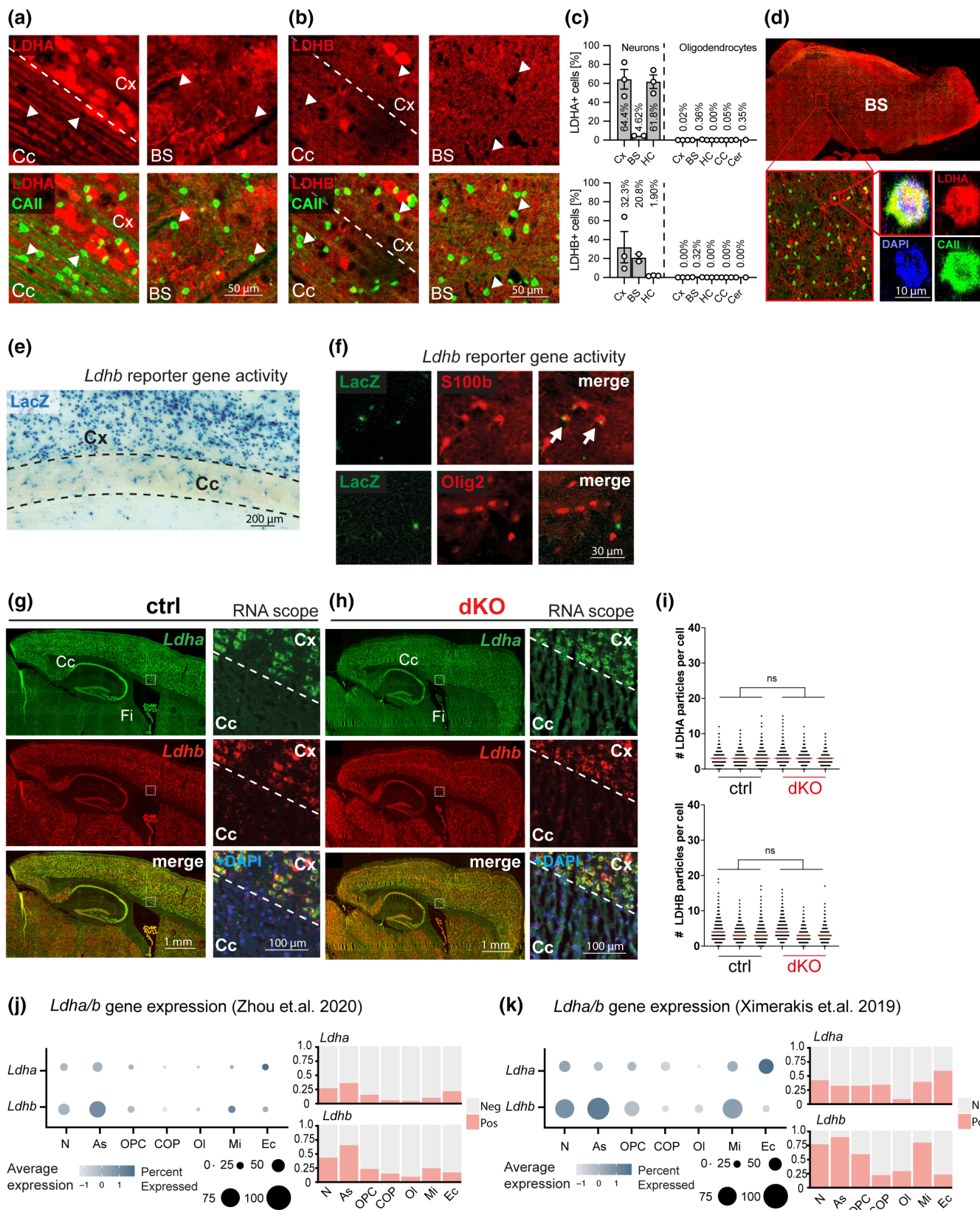


FIGURE 2 Legend on next page.

brain (Figures 2a–c, S2). The highest percentages of LDH-positive oligodendrocytes were detected in the brain stem not surpassing 0.5% (mean_{LDHA}: 0.36% ± 0.47%, mean_{LDHB}: 0.32% ± 0.12%; Figure 2c,d). An absence of LDHB expression from adult oligodendrocytes was also suggested by the LacZ reporter gene function in mice carrying a heterozygous ‘knockout-first’ *Ldhb*^{tm1a(KOMP)Wtsi} allele of the *Ldhb* gene (Figure 2e). X-gal staining was present in cortical neurons but weak in white matter tracts, including Corpus callosum (Figure 2e and data not shown). Here, immunohistochemical co-labeling revealed that LacZ expression was confined to astrocytes (Figure 2f).

To obtain independent confirmation, we performed RNAscope in situ hybridization of *Ldh* transcripts in brain sections from control and dKO mice at the age 6 months. Both *Ldha* and *Ldhb* mRNAs were detected in subsets of neurons throughout the brains of all genotypes. *Ldha* gene expression was strongest in the cerebral cortex and hippocampus as previously reported (Laughton et al., 2000; Ross et al., 2010) (Figure 2g). The more widely expressed *Ldhb* mRNA was also prominent in neurons of the basal forebrain, including several thalamic nuclei and in the midbrain as described (Laughton et al., 2000; Ross et al., 2010) (Figure 2g). *Ldha* and *Ldhb* mRNAs were of particularly low abundance in white matter tracts, such as Corpus callosum and hippocampal fimbria (Figure 2g,h). Importantly, mRNA levels were not further reduced in the conditional mutant mice (Figure 2i), which would be expected for nonsense mediated mRNA decay.

Lastly, we determined *Ldha* and *Ldhb* gene expression in major brain cell types by re-analyzing published single-cell resolution RNA sequencing data from mouse forebrain (Ximerakis et al., 2019; Zhou et al., 2020). We compared gene expression levels among clusters of neurons (N), astrocytes (As), microglia (Mi), and endothelial cells (Ec) with oligodendrocyte precursor cells (OPC), committed oligodendrocytes precursor cells (COP), and mature oligodendrocytes (OL). In both datasets, *Ldha* and *Ldhb* in particular, but also other glycolysis related genes were expressed

at a low rate in OLs in comparison to neurons and astrocytes (Figures 2j,k and S3a,b).

3.3 | LDHA in oligodendrocytes at developmental stages

During developmental myelination, oligodendrocytes are thought to import and utilize lactate for ATP generation and the synthesis of myelin lipids (Amaral et al., 2016; Rinholm et al., 2011; Sánchez-Abarca et al., 2001), which requires functional expression of LDH. In agreement, newly differentiated oligodendrocytes in culture express both LDHA and LDHB (Figure 3a). Moreover, when we analyzed the Corpus callosum at postnatal days (P)10, P15, P25 and P75 by immunohistochemistry, we detected LDHA in a gradually decreasing fraction of CC1-positive oligodendrocytes (slope = −30.4% ± 2.2%, $p < .001$, mean_{P10}: 92% ± 2.6%, mean_{P15}: 43% ± 9%, mean_{P25}: 16% ± 13%, mean_{P75}: 0% ± 0%; $n = 3-4$ per age; one-way ANOVA, post-test for trend; Figure 3b,f). Over this time course, also the LDHA expression level per cell decreased (Slope = −2.2% ± 0.6%, $p = .013$; $n = 3$ animals, one-way ANOVA with post-test for trend Figure 3b,g). LDHB was only marginally expressed in CC1⁺ oligodendrocytes at P10 (Figure 3c), too low to be reliably quantified. Our data suggest that the expression of LDHA is gradually downregulated with oligodendrocyte maturation. Whether the very few CA2 positive LDHA expressing oligodendrocytes detectable in the adult brain (Figure 2) represent immature cells is unclear.

If LDHA is expressed in oligodendrocytes during developmental myelination, it might also be involved in adult myelin repair. We thus assessed LDHA and LDHB expression during remyelination after 6 weeks of cuprizone-induced subcortical demyelination. Spontaneous remyelination was confirmed by immunohistochemical staining of PLP (Figure 3d). Indeed, 85 ± 4% of CC1⁺ cells in the re-myelinating Corpus callosum expressed LDHA at 6 weeks, a fraction similar to age

FIGURE 2 Very few oligodendrocytes in the adult brain express LDHA or LDHB. (a, b) By immunohistochemistry oligodendrocytes (CAII⁺ in green, arrowheads) in the cortex do largely not co-label for LDHA or LDHB (age 6 months). (c) Quantitative analyses of neurons (identified by NeuN expression) and oligodendrocytes (CAII⁺) co-expressing LDHA or LDHB in cortex (Cx), brain stem (BS), hippocampus (HC), Corpus callosum (CC), and cerebellum (Cer) at the age of 6 months ($n = 2-3$). (d) Rarely, single CAII⁺ oligodendrocytes or small clusters of CAII⁺ oligodendrocytes co-label for LDHA as depicted for the brain stem, and confirmed by confocal microscopy (bottom panels). (e) As revealed by X-gal staining (blue deposits) on brain sections of *Ldhb*^{tm1a(KOMP)Wtsi} mice, *Ldhb* promoter activity in the adult mouse Corpus callosum (Cc) is weak when compared to the overlaying gray matter (Cx) and (f) confined to S100b-labeled astrocytes (red) (X-gal staining pseudo colored in green). β -Galactosidase staining is absent from oligodendrocyte lineage cells identified by Olig2 expression (red). (g, h) Representative images of fluorescent RNAscope in situ hybridization for *Ldha* and *Ldhb* in the forebrain of controls and dKOs at age 6 months. Magnified images on the right illustrate *Ldha* and *Ldhb* positive neurons in the cortex (Cx) and similarly weak hybridization levels in the Corpus callosum (Cc) of controls (g) and mutants (h) (Fi, fimbria of the hippocampus). (i) Quantifications of fluorescent RNAscope in situ hybridization signals in dKO and control mice in the Corpus callosum resulted in equal numbers of detectable transcripts for *Ldha* (total observations = 5522 cells, $p = 0.307$; and *Ldhb* (total observations = 5522 cells, $p = .773$, 3 animals per genotype, linear mixed model with tukey post-hoc). (j, k) *Ldha* and *Ldhb* gene expression in neurons (N), astrocytes (As), oligodendrocyte precursor cells (OPC), differentiation committed oligodendrocytes precursors (COP), myelinating oligodendrocytes (OI), microglia (Mi), and endothelial cells (EC) were screened in wildtype animals from (j) Zhou et al., 2020 single-nuclei RNA sequencing (snRNA seq) dataset and (k) Ximerakis et al., 2019 single-cell RNA sequencing (scRNA seq) dataset. Dotplots visualize snRNA seq and scRNA seq expression data, respectively for *Ldha* and *Ldhb* within the given cell-type identity clusters. They provide information for the average expression level by color gradient, and percentages of cells that express each gene by size of the dot (Zhou et al., 2020: OI: *Ldha*, 6%; *Ldhb*: 11%; N: *Ldha*, 27%; *Ldhb*: 43%; As: *Ldha*, 36%, *Ldhb*, 65%. Ximerakis et al., 2019: OI: *Ldha*, 10%; *Ldhb*, 30%; N: *Ldha*, 43%; *Ldhb*: 76%; As: *Ldha*, 33%, *Ldhb*, 89%).

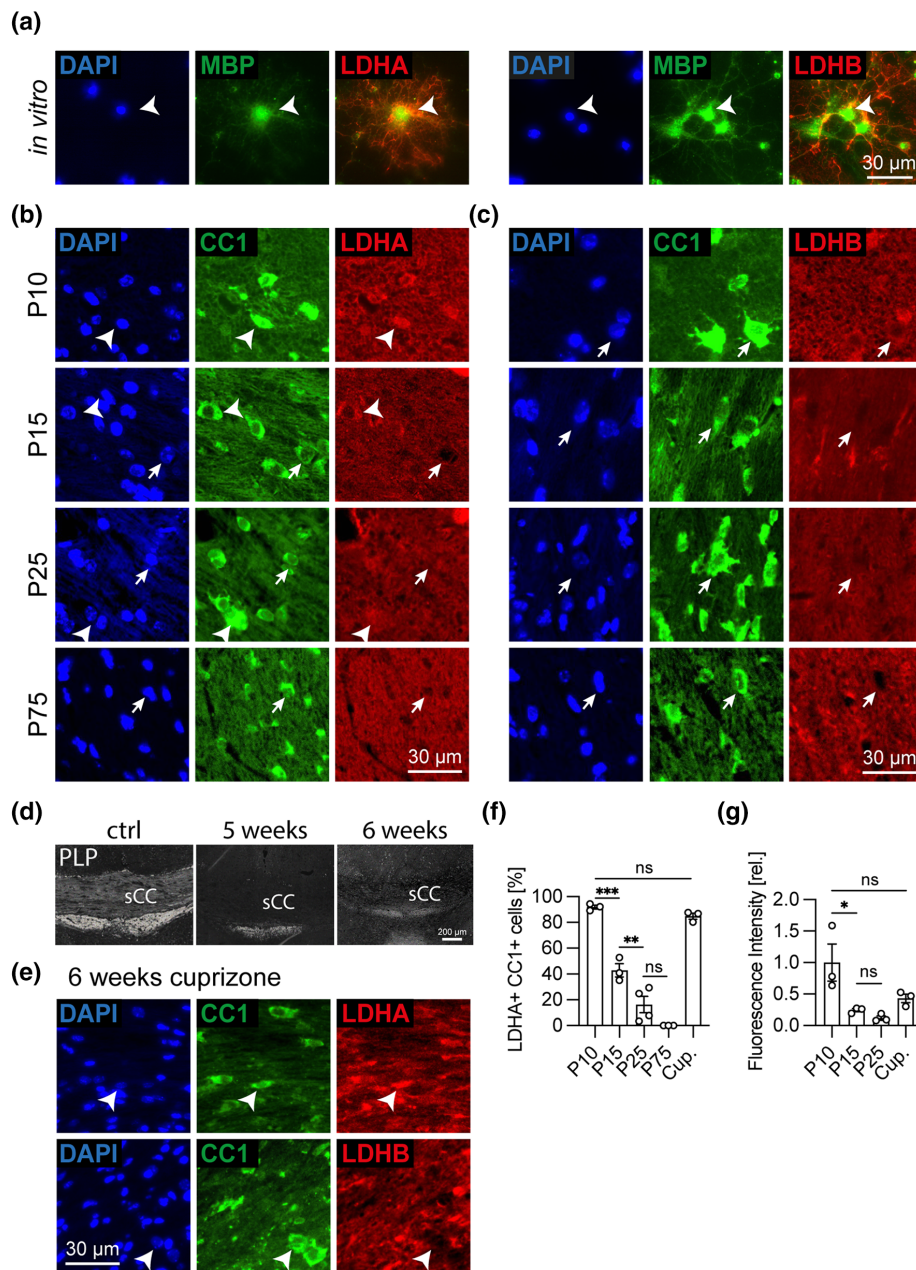


FIGURE 3 LDHA is transiently expressed during developmental myelination and during remyelination in the adult mouse brain. (a) Representative images of Magnetic Activated Cell Sorted (MACS) primary oligodendrocytes co-immunostained for MBP and either LDHA (left panel) or LDHB (right panel) 6 days after plating. (b) During the active phase of developmental myelination, a steadily decreasing number of CC1⁺ oligodendrocytes co-label for LDHA (arrow heads) in the Corpus callosum of mice at ages P10, P15, P25, and P75 (arrows indicate LDHA negative oligodendrocytes). (c) CC1⁺ oligodendrocytes (arrows) label at most very weakly for LDHB at P10 in the Corpus callosum. (d) Representative images of the splenium of the Corpus callosum (sCC) of untreated controls (left), mice treated with cuprizone for 5 weeks at the peak of demyelination (5 weeks, middle) and mice treated with cuprizone for 6 weeks during spontaneous remyelination (right). The sCC was assessed for myelin content by immunohistochemical analysis for PLP expression (white). (e) As addressed by immunohistochemistry, remyelinating CC1⁺ oligodendrocytes (green) at 6 weeks of cuprizone-treatment express LDHA (red) but not LDHB (red). (f) Quantification of the number of CC1⁺ oligodendrocytes that co-express LDHA in Corpus callosum during development (as shown by representative images in b) and at 6 weeks of cuprizone-treatment (as shown by representative images in e) indicates that oligodendrocytes transiently express LDHA during developmental myelination and induced remyelination ($F(4,11) = 5.837$, $p_{P10-P15} < 0.001$, $p_{P15-P25} = 0.004$, $p_{P25-P75} = 0.08$, $p_{P10-Cup} = 0.74$; one-way ANOVA, Šidák's multiple comparison test; $n = 3-4$ animals per condition). (g) Relative LDHA fluorescence intensity of CC1⁺ oligodendrocytes of the Corpus callosum normalized to P10 (set to 1) reveals that LDHA expression per cell is highest during beginning developmental myelination ($F(3,8) = 6.444$, $p_{P10-P15} = 0.02$, $p_{P15-P25} = 0.93$, $p_{P10-Cup} = 0.09$. one-way ANOVA, Šidák's multiple comparison test; $n = 3$ animals per condition with 20 averaged randomly selected LDHA⁺/CC1⁺ cells each). Asterisks represent significant differences with * $p < .05$; ** $p < .01$; *** $p < .001$; ns not significant. Cup, cuprizone.

(a) 24 mo senescence

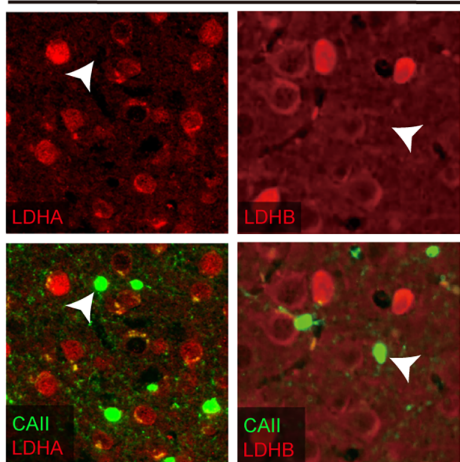
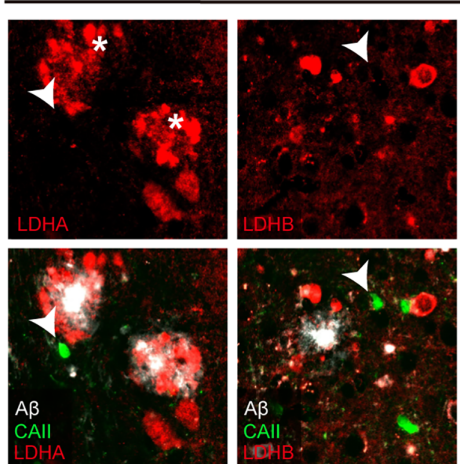
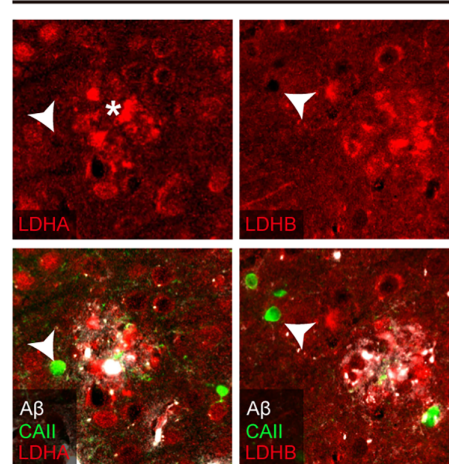
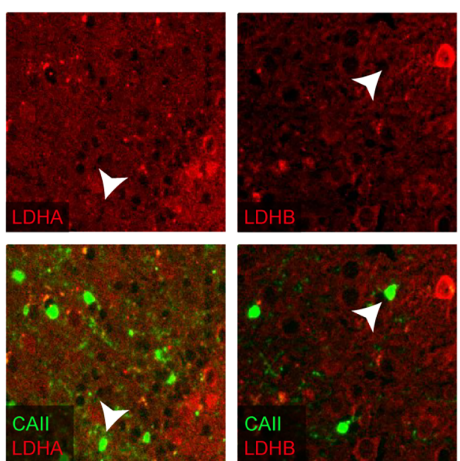
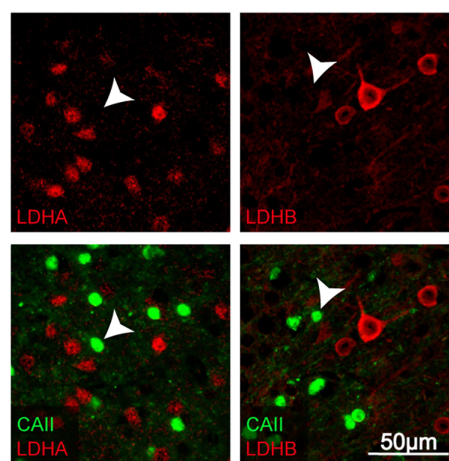
(b) 5x*FAD*(c) *App*^{NL-G-F}(d) *Plp* null(e) *Cox10* x *Cnp*^{Cre}

FIGURE 4 Oligodendroglial LDHA and LDHB expression is neither induced by aging, nor in mouse models of AD, in *Plp*^{null} mutants or in conditional *Cox10* mutants. Cortical oligodendrocytes labeled for CAII⁺ (green) (a) in the senescent brain (age, 24 mo), (b, c) in the vicinity to amyloid plaques (visualized by the anti- β -amyloid antibody 6E10, white) in 5x*FAD* brains (age, 6 mo), and *App*^{NLGF} brains (age, 6 mo), (d) in *Plp*^{null} mutant brains (age 6 mo), and (e) in oligodendroglial *Cox10* conditional mutant mice (age 9 mo) do not detectably co-express LDHA or LDHB (red). Note that the axonal swellings surrounding amyloid plaques (asterisks in b and c) are highly LDH positive. Images are representative of $n = 3$ animals per condition.

P10 (mean diff. = 7.2%, $CI_{95\%} = [-11.1\% \text{ to } 26.3\%]$, $p = .74$) while we observed no definite LDHB expression in these cells (Figure 3e,f). Expression levels of LDHA per cell were not significantly different from

age P10 (mean diff. = 2.9%, $CI_{95\%} = [-0.6\% \text{ to } 6.4\%]$, $p = .11$; Figure 3e,g). We conclude that during adult remyelination the development-like expression of oligodendroglial LDHA is recapitulated.

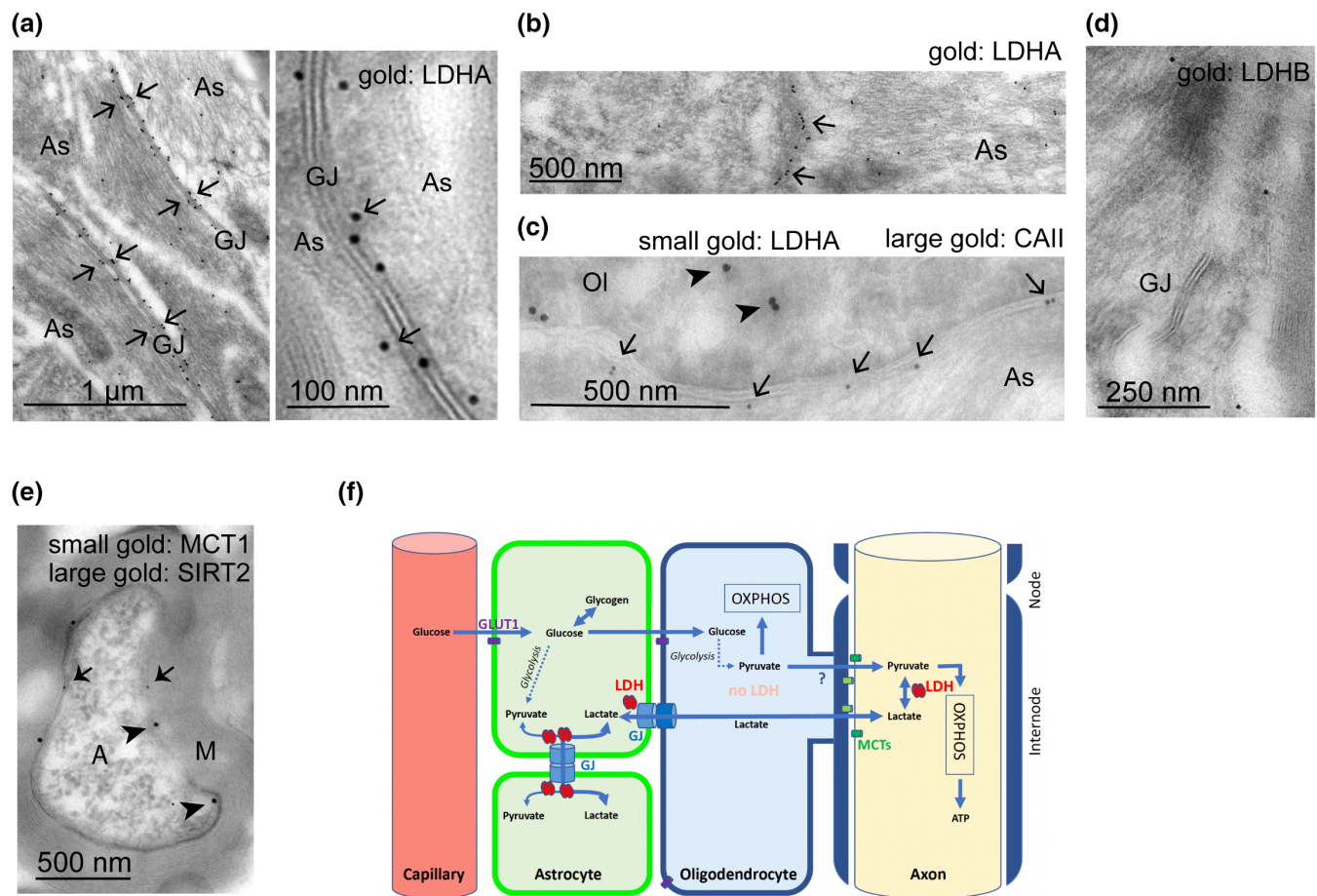


FIGURE 5 Colloidal immunogold-EM localization of LDHA along glial interfaces in ultrathin optic nerve sections of wildtype mice. (a) At 10 months of age and by immunodetection, LDHA (10 nm gold-particles, arrows) in astrocytes (As) is enriched at stretches of adjacent plasma membranes morphologically identified as gap junctions (GJ). (b) Adjacent plasma membranes of a LDHA positive astroglial process (identified by its high density of intermediate filaments) and a cell with very low or absent LDHA expression, possibly an oligodendrocyte. A stretch of LDHA immunolabeling (10 nm gold particles, arrows) is shown, in close apposition to the astroglial plasma membrane of the junction. (c) Presumed GJ between an oligodendrocyte (identified by CAll co-labeling, 15 nm gold particles, arrowheads) and an astrocyte, in which LDHA immunoreactivity (10 nm gold particles, arrows) accumulates close to the junction. (d) LDHB immunogold labeling (10 nm gold-particles, arrows) is present in astrocytes at 10 months of age. However, it is not enriched at gap junctions (GJ). (e) Co-immunodetection of SIRT2 (15 nm gold particles, arrowheads) and MCT1 (10 nm gold particles, arrows) in a myelinated axon. Note that both proteins localize to adaxonal myelin. A, axon; M, myelin. (f) Resulting working model of metabolic support in the optic nerve. Astrocytes (green) and axons (yellow) express both LDHA and LDHB. In astrocytes, pyruvate is generated by glycolysis and converted to lactate by LDHA that preferentially colocalizes with GAP junctions, which couple astrocytes among each other and with oligodendrocytes to form a panglial syncytium. Thus, oligodendrocytes may serve as funnels that pass astroglia-derived lactate to the axon, which is shielded over long distances by myelin from the extracellular space. Oligodendrocytes (blue) do not express LDHA and LDHB and thus neither generate lactate nor shuttle it back into their cellular metabolism. They may metabolically support axons with pyruvate instead.

3.4 | Oligodendroglial LDH expression in disease models and under metabolic stress

Brain aging and deficits of neuronal energy metabolism have been associated with elevated lactate (Cai et al., 2022; Ross et al., 2010). To determine whether these stressors directly affect oligodendroglial lactate metabolism, we analyzed LDHA and LDHB expression by immunohistochemistry in cortex and Corpus callosum of aged mice at 24 months (Figures 4a and S4a), in mouse models of Alzheimer's disease linked amyloidosis (5x*FAD*, *App*^{NLGf}) (Figures 4b,c and S4b,c),

and in PLP-deficient mice (Figures 4d and S4d), a model of spastic paraplegia type 2 (SPG2). None of these conditions were associated with an increased immunoreactivity of LDHA or LDHB in oligodendrocytes (Figures 4a–d and S4a–d). Even conditional *Cox10* mutant mice with perturbed oligodendroglial OXPHOS (Fünfschilling et al., 2012) did not detectably increase LDHA or LDHB expression in oligodendrocytes (Figures 4e and S4e). We conclude that mature oligodendrocytes in adult mice show no obvious adaptation of LDH expression and thus lactate metabolism when facing neurodegeneration and metabolic stress.

3.5 | LDHA is localized at astroglial gap junctions

Astrocytes form gap junctions (GJ) among themselves and with oligodendrocytes (Orthmann-Murphy et al., 2008). These coupled glial cells form a “panglial syncytium” (Giaume et al., 2021), in which metabolites such as pyruvate and lactate can pass from one cell to the other along concentration gradients. Interestingly, we found by immuno EM of optic nerves that astroglial LDHA (but not LDHB) is locally enriched at these GJ, including junctions that faced LDH-negative oligodendrocytes (Figure 5a–d). This enrichment of LDHA at GJ in combination with the localization of MCT1 at the inner tongue of myelin (Figure 5e) is compatible with a model that astrocytes “funnel” lactate through oligodendrocytes and the cytosolic myelin compartment to axons, whereas oligodendrocytes might deliver self-generated pyruvate to the axonal compartment (Figure 5f).

4 | DISCUSSION

We report the surprising observation that oligodendrocytes in the adult mouse brain lack expression of LDHA and LDHB, at least at the expected level if oligodendroglial lactate were the main glial metabolite that supports axonal energy metabolism. This opens the possibility that glycolytic oligodendrocytes, which are suggested to support electrically active axons with an excess of glycolysis products (Fünfschilling et al., 2012; Lee et al., 2012; Saab et al., 2016; Trevisiol et al., 2017) do so primarily by self-made pyruvate. This may distinguish oligodendrocytes from astrocytes that express LDH and reportedly use a “lactate shuttle” to directly support the synaptic energy metabolism in cortical gray matter (Magistretti & Allaman, 2018; Pellerin & Magistretti, 1994). Additionally, we report here that LDHA but not LDHB is enriched at GJ between astrocytes and at the astroglial side of astrocyte-oligodendrocyte junctions in optic nerves. Our data are thus compatible with a revised working model of Fünfschilling et al. (2012), in which lactate is preferentially produced in astrocytes close to their gap junctions with neighboring cells, and in which myelinic channels funnel astroglial lactate and oligodendroglial pyruvate to the periaxonal space of myelinated internodes.

Our findings of negligible LDH expression in mature oligodendrocytes are supported by several lines of evidence. These include X-gal reporter gene expression analysis, and LDH protein and mRNA localization data, and are in good agreement with the absence of detectable pathology in *Ldha*^{flox/flox};*Ldhb*^{flox/flox};*PlpCreERT2* mice. Also, the re-analyses of snRNAseq and scRNAseq data from wildtype mice (Ximerakis et al., 2019; Zhou et al., 2020) suggest that both *Ldh* transcripts are expressed markedly less in mature myelinating oligodendrocytes compared to neurons and astrocytes (Figure 2j,k). Interestingly, metabolic stress that increases glycolytic metabolism and LDHA expression in other systems, including mitochondrial dysfunction in mice with *Cox10*-deficiency in neurons or Müller cells (Garcia et al., 2022; Nsiah & Inman, 2022), did not induce LDH expression in mature *Cox10*-deficient oligodendrocytes (Figure 4e), revealing a remarkable lack of metabolic plasticity.

In contrast, and in agreement with prior reports of cultured oligodendrocytes utilizing lactate as an energy source (Amaral et al., 2016; Rinholm et al., 2011; Sánchez-Abarca et al., 2001), we detected both LDHA and LDHB in these cells in vitro. Nevertheless, in vivo evidence for the use of lactate during developmental myelination is lacking. Concordantly, we found that in vivo only LDHA but not LDHB was robustly expressed in immature oligodendrocytes during postnatal development and, similarly, during the repair of demyelinated lesions. Since LDH tetramers with a surplus of LDHA subunits are biased toward the generation of lactate (Claps et al., 2022; Mishra & Banerjee, 2019) these findings rather argue in favor of the production and release of lactate from immature oligodendrocytes under these conditions.

For regenerating the electron acceptor NAD⁺ from NADH, the LDH reaction is the expected pathway for cells that highly rely on sustained aerobic glycolysis (Parra-Bonilla et al., 2010; Rajala et al., 2023; Sheppard et al., 2021; Valvona et al., 2016). Hence, it was surprising that mature oligodendrocytes expressed LDH at negligible amounts and did not increase its expression when mitochondrial electron transport chain was perturbed in oligodendroglial *Cox10* mutants. This may be best explained by sufficient OXPHOS activity in wildtype oligodendrocytes to regenerate NAD⁺ and even residual activity in the absence of *Cox10*. Residual OXPHOS activity has been hypothesized for other celltype-specific *Cox10* mutant mice (Baek et al., 2018; Diaz et al., 2005) and in a human patient with a homozygous mutation in the *COX10* start codons (Coenen et al., 2004). With respect to alternative pathways of cellular NAD⁺ regeneration, we further note that oligodendrocytes are reportedly the only cells in the brain that express cytosolic glycerol-3-phosphate-dehydrogenase (GPD1) (Cheng et al., 1997; Leveille et al., 1980; Nguyen et al., 2003). This enzyme catalyzes the reversible conversion of dihydroxyacetone phosphate (DHAP) to glycerol-3-phosphate (G3P) by oxidizing NADH to NAD⁺. Since GPD1 connects glycolysis to lipid metabolism (Sato et al., 2020) oligodendrocytes may benefit from coupling the regeneration of NAD⁺ to the generation of G3P as a phospholipid precursor in lipid biosynthesis. Cytosolic GPD1 in oligodendrocytes may thus provide an additional way to make NAD⁺ regeneration partly independent from the action of mitochondrial NADH shuttles and may thus substitute for the lack of LDH reaction in oligodendrocytes to a certain extent. Interestingly, increased glycolysis and GPD1 activity are likewise reported to be coupled through cytosolic NAD⁺ recycling in kidney (Zhou et al., 2023).

In a previous study (Fünfschilling et al., 2012), we had measured an increased abundance of lactate in the brains of *Cox10*^{fl/fl};*Cnp*^{Cre} mice. These findings were indirect evidence for an elevated rate of glycolysis in oligodendrocytes and myelin in response to genetically perturbed OXPHOS. However, in order to be detectable, both normal and elevated lactate signals required in addition the transient and unspecific inhibition of OXPHOS by the volatile anesthetic isoflurane (Fünfschilling et al., 2012). Following the removal of isoflurane, lactate dropped to undetectable levels in NMR spectroscopy in both *Cox10* conditional mutants and control brains. This supported the working model that electrical activity and regained OXPHOS in the neuronal compartment lead to rapidly metabolizing any accumulated, glial-

derived glycolysis products. It also provided indirect evidence for a physical shuttling of glycolysis products from mutant oligodendrocytes to OXPPOS capable neurons and their axons, which can consume either pyruvate or lactate as a metabolic fuel (Saab & Nave, 2017). However, we could not decide at the time whether oligodendrocytes deliver primarily lactate or pyruvate (Fünfschilling et al., 2012). Given the low levels of LDH in oligodendrocytes, we can refine our model and hypothesize that it is predominantly oligodendrocyte-derived pyruvate, which enters the axonal compartment. Similar to lactate, an excess of pyruvate, the primary end-product of glycolysis in oligodendrocytes, can freely diffuse to the axonal compartment via myelinic nanochannels (Edgar et al., 2021) and be transported by monocarboxylate transporters MCT1 and MCT2. This would implicate that elevated brain lactate measured in *Cox10^{fl/fl};Cnp^{Cre/wt}* mice had secondarily built up within the LDH-positive axonal compartments in response to the influx of oligodendrocyte-derived pyruvate.

We must, however, also consider that *Cnp^{Cre}* mediated neuronal off-target recombination can be detected in subsets of forebrain neurons (Jo et al., 2021; Tognatta et al., 2017) (Figure S1) and may thus have contributed to the observed axonal lactate peaks in *Cox10^{fl/fl};Cnp^{Cre}* mice. Notably, neurons have been recently shown to enhance their own glycolysis, LDHA expression and consequently lactate production as an adaptive metabolic response to neuron-specific *Cox10* deficiency (Garcia et al., 2022). However, we note that neuropathology, which follows with a certain delay time the targeted disruption of neuronal *Cox10* (Diaz et al., 2012), was not detected in *Cox10^{fl/fl};Cnp^{Cre}* mice (Fünfschilling et al., 2012).

Astrocytes and oligodendrocytes, which are coupled by GJ (Orthmann-Murphy et al., 2008), form a “panglial” network of cells that spans from the blood brain barrier to the periaxonal space of the myelinated axons. The enrichment of LDH at gap junctions of adjacent astrocytes and at the astroglial aspect of astrocyte-to-oligodendrocyte junctions in the optic nerve is compatible with the hypothesis that glycolysis products of astrocytes, generated quickly from glycogen stores upon acute energetic demands, are shuttled as lactate via oligodendrocytes/myelin into the axonal compartment. The preferential localization of LDHA at all identified astroglial gap junctions would allow these cells to efficiently regain NAD⁺ as the glycolytic end products are released (Figure 5). The extremely low level of LDH in oligodendrocytes themselves most likely prevents further metabolization of lactate before it has reached the axonal compartment. Thus, we hypothesize that oligodendrocytes and myelin also provide the space and architecture for astroglial lactate to diffuse towards the axon, essentially as a “funnel” for glycolysis products. A similar assisting role of oligodendrocytes has been hypothesized for the thalamus (Philippot et al., 2021).

Taken together, the lack of LDH in oligodendrocytes suggests a revised working model for white matter energy metabolism (Figure 5f), in which the unequal distribution of LDH facilitates the efficient transport of glycolysis products between astrocytes, oligodendrocytes, and the axonal compartment.

AUTHOR CONTRIBUTIONS

ES and SG conceptualized and designed the study. ES, BZ, KK, and SG generated mouse lines, performed histology, microscopy, in situ hybridization, biochemical experiments, and statistical analyses. TS re-analyzed published RNA-seq datasets. EA helped with histological analyses. SBS prepared primary oligodendrocytes cultures. CD established 5xFAD and App^{NLGF} mutants and provided brain sections of PLP deficient mice. HBW and KK generated and established the *Ldha^{flox/flox};Ldhb^{flox/flox};CNP^{Cre/+}* mouse line. GS performed cuprizone-induced demyelination and remyelination experiments. JH provided critical conceptual input. WM performed EM analyses. ES and SG wrote the manuscript and created figures. KAN edited the manuscript. All authors were involved in the revision of the draft manuscript and have agreed to the final content.

ACKNOWLEDGMENTS

We thank Ulli Bode, Torben Ruhwedel, Boguslawa Sadowski, Annette Fahrenholz, and Ursula Kutzke for technical assistance, Ursula Fünfschilling and Lotti Supplies for brain paraffin sections of *Cox10* mutant mice and respective controls, Said Ghandour, Charles Stiles and John Alberta for antibodies, and all personnel of the animal facility of the Max Planck Institute for Multidisciplinary Sciences (MPI-NAT), City Campus for animal husbandry. This work was supported by the ERC Advanced Investigators Grant MyelinANO (K.-A.N.), the German Research Foundation grant SPP1757 (GS, SG), and the Dr. Myriam and Sheldon Adelson Medical Foundation (AMRF). Open Access funding enabled and organized by Projekt DEAL.

CONFLICT OF INTEREST STATEMENT

The authors declare no conflict of interest.

DATA AVAILABILITY STATEMENT

The data that support the findings of this study are available from the corresponding author upon reasonable request.

ORCID

Kathrin Kusch  <https://orcid.org/0000-0002-5079-502X>

Gesine Saher  <https://orcid.org/0000-0003-3507-9604>

Johannes Hirrlinger  <https://orcid.org/0000-0002-6327-0089>

Sandra Goebbels  <https://orcid.org/0000-0001-8343-9972>

REFERENCES

- Albanese, M., Zagaglia, S., Landi, D., Boffa, L., Nicoletti, C. G., Marciani, M. G., Mandolesi, G., Marfia, G. A., Buttari, F., Mori, F., & Centonze, D. (2016). Cerebrospinal fluid lactate is associated with multiple sclerosis disease progression. *Journal of Neuroinflammation*, 13(1), 36. <https://doi.org/10.1186/S12974-016-0502-1>
- Allaman, I., Bélanger, M., & Magistretti, P. J. (2011). Astrocyte-neuron metabolic relationships: For better and for worse. *Trends in Neurosciences*, 34(2), 76–87. <https://doi.org/10.1016/J.TINS.2010.12.001>
- Amaral, A. I., Hadera, M. G., Tavares, J. M., Kotter, M. R. N., & Sonnewald, U. (2016). Characterization of glucose-related metabolic pathways in differentiated rat oligodendrocyte lineage cells. *Glia*, 64(1), 21–34. <https://doi.org/10.1002/GLIA.22900>



- Amaral, A. I., Meisingset, T. W., Kotter, M. R., & Sonnewald, U. (2013). Metabolic aspects of neuron-oligodendrocyte-astrocyte interactions. *Frontiers in Endocrinology*, 4(MAY), 54. <https://doi.org/10.3389/FENDO.2013.00054/BIBTEX>
- Baek, J.-H., Gomez, I. G., Wada, Y., Roach, A., Mahad, D., & Duffield, J. S. (2018). Deletion of the mitochondrial complex-IV cofactor heme A: Farnesyltransferase causes focal segmental glomerulosclerosis and interferon response. *The American Journal of Pathology*, 188(12), 2745–2762. <https://doi.org/10.1016/j.ajpath.2018.08.018>
- Berghoff, S. A., Düking, T., Spieth, L., Winchenbach, J., Stumpf, S. K., Gerndt, N., Kusch, K., Ruhwedel, T., Möbius, W., & Saher, G. (2017). Blood-brain barrier hyperpermeability precedes demyelination in the cuprizone model. *Acta Neuropathologica Communications*, 5(1), 94. <https://doi.org/10.1186/S40478-017-0497-6>
- Bloom, A. J., Hackett, A. R., Strickland, A., Yamada, Y., Ippolito, J., Schmidt, R. E., Sasaki, Y., DiAntonio, A., & Milbrandt, J. (2022). Disruption of lactate metabolism in the peripheral nervous system leads to motor-selective deficits (p. 2022.06.29.497865). *bioRxiv*. <https://doi.org/10.1101/2022.06.29.497865>
- Bosoi, C. R., & Rose, C. F. (2014). Elevated cerebral lactate: Implications in the pathogenesis of hepatic encephalopathy. *Metabolic Brain Disease*, 29(4), 919–925. <https://doi.org/10.1007/S11011-014-9573-9>
- Bouzier-Sore, A. K., Voisin, P., Canioni, P., Magistretti, P. J., & Pellerin, L. (2003). Lactate is a preferential oxidative energy substrate over glucose for neurons in culture. *Journal of Cerebral Blood Flow and Metabolism: Official Journal of the International Society of Cerebral Blood Flow and Metabolism*, 23(11), 1298–1306. <https://doi.org/10.1097/O1.WCB.0000091761.61714.25>
- Brown, A. M., Tekkök, S. B., & Ransom, B. R. (2004). Energy transfer from astrocytes to axons: The role of CNS glycogen. *Neurochemistry International*, 45(4), 529–536. <https://doi.org/10.1016/j.neuint.2003.11.005>
- Cai, M., Wang, H., Song, H., Yang, R., Wang, L., Xue, X., Sun, W., & Hu, J. (2022). Lactate is answerable for brain function and treating brain diseases: Energy substrates and signal molecules. *Frontiers in Nutrition*, 9, 800901. <https://doi.org/10.3389/fnut.2022.800901>
- Cheng, J. D., Zhao, P., De Los, E., Monteros, A., & De Vellis, J. (1997). Glial and fat-specific expression of the rat glycerol phosphate dehydrogenase-luciferase fusion gene in transgenic mice. *Journal of Neuroscience Research*, 50, 300–311. [https://doi.org/10.1002/\(SICI\)1097-4547\(19971015\)50:2](https://doi.org/10.1002/(SICI)1097-4547(19971015)50:2)
- Claps, G., Faouzi, S., Quidville, V., Chehade, F., Shen, S., Vagner, S., & Robert, C. (2022). The multiple roles of LDH in cancer. *Nature Reviews Clinical Oncology* 2022 19:12, 19(12), 749–762. <https://doi.org/10.1038/s41571-022-00686-2>
- Coenen, M. J. H., van den Heuvel, L. P., Ugalde, C., Ten Brinke, M., Nijtmans, L. G. J., Trijbels, F. J. M., Beblo, S., Maier, E. M., Muntau, A. C., & Smeitink, J. A. M. (2004). Cytochrome c oxidase biogenesis in a patient with a mutation in COX10 gene. *Annals of Neurology*, 56(4), 560–564. <https://doi.org/10.1002/ana.20229>
- Diaz, F., Garcia, S., Padgett, K. R., & Moraes, C. T. (2012). A defect in the mitochondrial complex III, but not complex IV, triggers early ROS-dependent damage in defined brain regions. *Human Molecular Genetics*, 21(23), 5066–5077. <https://doi.org/10.1093/hmg/dds350>
- Diaz, F., Thomas, C. K., Garcia, S., Hernandez, D., & Moraes, C. T. (2005). Mice lacking COX10 in skeletal muscle recapitulate the phenotype of progressive mitochondrial myopathies associated with cytochrome c oxidase deficiency. *Human Molecular Genetics*, 14(18), 2737–2748. <https://doi.org/10.1093/hmg/ddi307>
- Dienel, G. A. (2017). Lack of appropriate stoichiometry: Strong evidence against an energetically important astrocyte-neuron lactate shuttle in brain. *Journal of Neuroscience Research*, 95(11), 2103–2125. <https://doi.org/10.1002/jnr.24015>
- Edgar, J. M., McGowan, E., Chapple, K. J., Möbius, W., Lemgruber, L., Insall, R. H., Nave, K.-A., & Boullenger, A. (2021). Río-Hortega's drawings revisited with fluorescent protein defines a cytoplasm-filled channel system of CNS myelin. *Journal of Anatomy*, 239(6), 1241–1255. <https://doi.org/10.1111/joa.13577>
- Fünfschilling, U., Supplie, L. M., Mahad, D., Boretius, S., Saab, A. S., Edgar, J., Brinkmann, B. G., Kassmann, C. M., Tzvetanova, I. D., Möbius, W., Diaz, F., Meijer, D., Suter, U., Hamprecht, B., Sereda, M. W., Moraes, C. T., Frahm, J., Goebbels, S., & Nave, K. A. (2012). Glycolytic oligodendrocytes maintain myelin and long-term axonal integrity. *Nature*, 485(7399), 517–521. <https://doi.org/10.1038/NATURE11007>
- Gallyas, F. (1979). Silver staining of myelin by means of physical development. *Neurological Research*, 1(2), 203–209. <https://doi.org/10.1080/01616412.1979.11739553>
- Garcia, S., Saldana-Caboverde, A., Anwar, M., Raval, A. P., Nissanka, N., Pinto, M., Moraes, C. T., & Diaz, F. (2022). Enhanced glycolysis and GSK3 inactivation promote brain metabolic adaptations following neuronal mitochondrial stress. *Human Molecular Genetics*, 31(5), 692–704. <https://doi.org/10.1093/HMG/DDAB282>
- Genoud, S., Lappe-Siefke, C., Goebbels, S., Radtke, F., Aguet, M., Scherer, S. S., Suter, U., Nave, K. A., & Mantei, N. (2002). Notch1 control of oligodendrocyte differentiation in the spinal cord. *The Journal of Cell Biology*, 158(4), 709–718. <https://doi.org/10.1083/JCB.200202002>
- Giaume, C., Naus, C. C., Sáez, J. C., & Leybaert, L. (2021). Glial connexins and pannexins in the healthy and diseased brain. *Physiological Reviews*, 101(1), 93–145. <https://doi.org/10.1152/PHYSREV.00043.2018/ASSET/IMAGES/LARGE/Z9J0042029570010.JPEG>
- Goldberg, E., Eddy, E. M., Duan, C., & Odet, F. (2010). LDHC: The ultimate testis-specific gene. *Journal of Andrology*, 31(1), 86–94. <https://doi.org/10.2164/jandrol.109.008367>
- Hao, Y., Hao, S., Andersen-Nissen, E., Mauck, W. M., Zheng, S., Butler, A., Lee, M. J., Wilk, A. J., Darby, C., Zager, M., Hoffman, P., Stoeckius, M., Papalex, E., Mimitou, E. P., Jain, J., Srivastava, A., Stuart, T., Fleming, L. M., Yeung, B., ... Satija, R. (2021). Integrated analysis of multimodal single-cell data. *Cell*, 184(13), 3573–3587.e29. <https://doi.org/10.1016/j.cell.2021.04.048>
- Hirrlinger, P. G., Scheller, A., Braun, C., Hirrlinger, J., & Kirchhoff, F. (2006). Temporal control of gene recombination in astrocytes by transgenic expression of the tamoxifen-inducible DNA recombinase variant CreERT2. *Glia*, 54(1), 11–20. <https://doi.org/10.1002/GLIA.20342>
- Jo, Y. R., Kim, H. R., Jang, S. Y., Go, H., Song, M.-Y., Park, D. K., Oh, Y., Jo, J., Shin, Y. K., Lee, S. J., Cheon, S.-M., Lee, H. K., Lee, K. E., Kim, Y. H., & Park, H. T. (2021). Potential neuron-autonomous Purkinje cell degeneration by 2',3'-cyclic nucleotide 3'-phosphodiesterase promoter/Cre-mediated autophagy impairments. *The FASEB Journal*, 35(1), e21225. <https://doi.org/10.1096/fj.202001366RR>
- Joseph, S., Werner, H. B., & Stegmüller, J. (2019). Gallyas silver impregnation of myelinated nerve fibers. *Bio-Protocol*, 9(22), e3436. <https://doi.org/10.21769/BioProtoc.3436>
- Karagiannis, A., Gallopini, T., Lacroix, A., Plaisier, F., Piquet, J., Geoffroy, H., Hepp, R., Naude, J., Le Gac, B., Egger, R., Lambalez, B., Li, D., Rossier, J., Staiger, J. F., Imamura, H., Seino, S., Roeper, J., & Cauli, B. (2021). Lactate is an energy substrate for rodent cortical neurons and enhances their firing activity. *eLife*, 10, e71424. <https://doi.org/10.7554/ELIFE.71424>
- Klugmann, M., Schwab, M. H., Pühlhofer, A., Schneider, A., Zimmermann, F., Griffiths, I. R., & Nave, K. A. (1997). Assembly of CNS myelin in the absence of proteolipid protein. *Neuron*, 18(1), 59–70. [https://doi.org/10.1016/S0896-6273\(01\)80046-5](https://doi.org/10.1016/S0896-6273(01)80046-5)
- Kopperschlager, G., & Kirchberger, J. (1996). Methods for the separation of lactate dehydrogenases and clinical significance of the enzyme. *Journal of Chromatography. B, Biomedical Applications*, 684(1–2), 25–49. [https://doi.org/10.1016/0378-4347\(96\)00133-8](https://doi.org/10.1016/0378-4347(96)00133-8)
- Lappe-Siefke, C., Goebbels, S., Gravel, M., Nicksch, E., Lee, J., Braun, P. E., Griffiths, I. R., & Nave, K. A. (2003). Disruption of Cnp1 uncouples

- oligodendroglial functions in axonal support and myelination. *Nature Genetics*, 33(3), 366–374. <https://doi.org/10.1038/NG1095>
- Laughton, J. D., Charnay, Y., Belloir, B., Pellerin, L., Magistretti, P. J., & Bouras, C. (2000). Differential messenger RNA distribution of lactate dehydrogenase LDH-1 and LDH-5 isoforms in the rat brain. *Neuroscience*, 96(3), 619–625. [https://doi.org/10.1016/S0306-4522\(99\)00580-1](https://doi.org/10.1016/S0306-4522(99)00580-1)
- Lee, Y., Morrison, B. M., Li, Y., Lengacher, S., Farah, M. H., Hoffman, P. N., Liu, Y., Tsingalia, A., Jin, L., Zhang, P. W., Pellerin, L., Magistretti, P. J., & Rothstein, J. D. (2012). Oligodendroglia metabolically support axons and contribute to neurodegeneration. *Nature*, 487(7408), 443–448. <https://doi.org/10.1038/nature11314>
- Leone, D. P., Genoud, S., Atanasoski, S., Grausenburger, R., Berger, P., Metzger, D., Macklin, W. B., Chambon, P., & Suter, U. (2003). Tamoxifen-inducible glia-specific Cre mice for somatic mutagenesis in oligodendrocytes and Schwann cells. *Molecular and Cellular Neuroscience*, 22(4), 430–440. [https://doi.org/10.1016/S1044-7431\(03\)00029-0](https://doi.org/10.1016/S1044-7431(03)00029-0)
- Leveille, P. J., McGinnis, J. F., Maxwell, D. S., & De Vellis, J. (1980). Immunocytochemical localization of glycerol-3-phosphate dehydrogenase in rat oligodendrocytes. *Brain Research*, 196(2), 287–305. [https://doi.org/10.1016/0006-8993\(80\)90397-2](https://doi.org/10.1016/0006-8993(80)90397-2)
- Liguori, C., Stefani, A., Sancesario, G., Sancesario, G. M., Marciari, M. G., & Pierantozzi, M. (2015). CSF lactate levels, τ proteins, cognitive decline: A dynamic relationship in Alzheimer's disease. *Journal of Neurology, Neurosurgery, and Psychiatry*, 86(6), 655–659. <https://doi.org/10.1136/JNNP-2014-308577>
- Mächler, P., Wyss, M. T., Elsayed, M., Stobart, J., Gutierrez, R., Von Faber-Castell, A., Kaelin, V., Zuend, M., San Martín, A., Romero-Gómez, I., Baeza-Lehnert, F., Lengacher, S., Schneider, B. L., Aebischer, P., Magistretti, P. J., Barros, L. F., & Weber, B. (2016). In vivo evidence for a lactate gradient from astrocytes to neurons. *Cell Metabolism*, 23(1), 94–102. <https://doi.org/10.1016/J.CMET.2015.10.010>
- Madsen, P. M., Motti, D., Karmally, S., Szymkowski, D. E., Lamberts, K. L., Bethea, J. R., & Brambilla, R. (2016). Oligodendroglial TNFR2 mediates membrane TNF-dependent repair in experimental autoimmune encephalomyelitis by promoting oligodendrocyte differentiation and remyelination. *The Journal of Neuroscience: The Official Journal of the Society for Neuroscience*, 36(18), 5128–5143. <https://doi.org/10.1523/JNEUROSCI.0211-16.2016>
- Magistretti, P. J., & Allaman, I. (2018). Lactate in the brain: From metabolic end-product to signalling molecule. *Nature Reviews Neuroscience*, 19(4), Article 4–Article 249. <https://doi.org/10.1038/nrn.2018.19>
- Mishra, D., & Banerjee, D. (2019). Lactate dehydrogenases as metabolic links between tumor and stroma in the tumor microenvironment. *Cancers*, 11(6), 750. <https://doi.org/10.3390/CANCERS11060750>
- Miura, S. (1966a). Lactic dehydrogenase isozymes of the brain. I. Electrophoretic studies on regional distribution and ontogenesis. *Folia Psychiatrica et Neurologica Japonica*, 20(4), 337–347. <https://doi.org/10.1111/J.1440-1819.1966.TB02647.X>
- Miura, S. (1966b). Lactic dehydrogenase isozymes of the brain. II. Distribution in the mitochondrial fraction of the rat brain. *Folia Psychiatrica et Neurologica Japonica*, 20(4), 349–359. <https://doi.org/10.1111/J.1440-1819.1966.TB02648.X>
- Nave, K. A. (2010). Myelination and support of axonal integrity by glia. *Nature*, 468(7321), 244–252. <https://doi.org/10.1038/NATURE09614>
- Nguyen, N. H. T., Bräthe, A., & Hassel, B. (2003). Neuronal uptake and metabolism of glycerol and the neuronal expression of mitochondrial glycerol-3-phosphate dehydrogenase. *Journal of Neurochemistry*, 85(4), 831–842. <https://doi.org/10.1046/J.1471-4159.2003.01762.X>
- Nsiah, N. Y., & Inman, D. M. (2022). Destabilizing COXIV in Müller glia increases retinal glycolysis and alters scotopic electroretinogram. *Cell*, 11(23), 3756. <https://doi.org/10.3390/cells11233756>
- Oakley, H., Cole, S. L., Logan, S., Maus, E., Shao, P., Craft, J., Guillozet-Bongaarts, A., Ohno, M., Disterhoft, J., Van Eldik, L., Berry, R., & Vassar, R. (2006). Intraneuronal beta-amyloid aggregates, neurodegeneration, and neuron loss in transgenic mice with five familial Alzheimer's disease mutations: Potential factors in amyloid plaque formation. *The Journal of Neuroscience: The Official Journal of the Society for Neuroscience*, 26(40), 10129–10140. <https://doi.org/10.1523/JNEUROSCI.1202-06.2006>
- Obel, L. F., Müller, M. S., Walls, A. B., Sickmann, H. M., Bak, L. K., Waagepetersen, H. S., & Schousboe, A. (2012). Brain glycogen-new perspectives on its metabolic function and regulation at the subcellular level. *Frontiers in Neuroenergetics*, 4(MAR), 3. <https://doi.org/10.3389/FNENE.2012.00003>
- Orthmann-Murphy, J. L., Abrams, C. K., & Scherer, S. S. (2008). Gap junctions couple astrocytes and oligodendrocytes. *Journal of Molecular Neuroscience*, 35, 101–116. <https://doi.org/10.1007/s12031-007-9027-5>
- Parra-Bonilla, G., Alvarez, D. F., Al-Mehdi, A. B., Alexeyev, M., & Stevens, T. (2010). Critical role for lactate dehydrogenase in aerobic glycolysis that sustains pulmonary microvascular endothelial cell proliferation. *American Journal of Physiology. Lung Cellular and Molecular Physiology*, 299(4), L513–L522. <https://doi.org/10.1152/AJPLUNG.00274.2009>
- Pellerin, L., & Magistretti, P. J. (1994). Glutamate uptake into astrocytes stimulates aerobic glycolysis: A mechanism coupling neuronal activity to glucose utilization. *Proceedings of the National Academy of Sciences of the United States of America*, 91(22), 10625–10629. <https://doi.org/10.1073/PNAS.91.22.10625>
- Pellerin, L., & Magistretti, P. J. (2004). Neuroscience. Let there be (NADH) light. *Science*, 305(5680), 50–52. <https://doi.org/10.1126/SCIENCE.1100428>
- Pellerin, L., & Magistretti, P. J. (2012). Sweet sixteen for ANLS. *Journal of Cerebral Blood Flow and Metabolism: Official Journal of the International Society of Cerebral Blood Flow and Metabolism*, 32(7), 1152–1166. <https://doi.org/10.1038/JCBFM.2011.149>
- Peters, P. J., & Pierson, J. (2008). Immunogold labeling of thawed cryosections. *Methods in Cell Biology*, 88, 131–149. [https://doi.org/10.1016/S0091-679X\(08\)00408-1](https://doi.org/10.1016/S0091-679X(08)00408-1)
- Philippot, C., Griemsmann, S., Jabs, R., Seifert, G., Kettenmann, H., & Steinhäuser, C. (2021). Astrocytes and oligodendrocytes in the thalamus jointly maintain synaptic activity by supplying metabolites. *Cell Reports*, 34(3), 108642. <https://doi.org/10.1016/J.CELREP.2020.108642>
- Philips, T., Mironova, Y. A., Jouroukhin, Y., Chew, J., Vidensky, S., Farah, M. H., Pletnikov, M. V., Bergles, D. E., Morrison, B. M., & Rothstein, J. D. (2021). MCT1 deletion in oligodendrocyte lineage cells causes late-onset hypomyelination and axonal degeneration. *Cell Reports*, 34(2), 108610. <https://doi.org/10.1016/J.CELREP.2020.108610>
- Rajala, A., Bhat, M. A., Teel, K., Gopinadhan Nair, G. K., Purcell, L., & Rajala, R. V. S. (2023). The function of lactate dehydrogenase in retinal neurons: Implications to retinal degenerative diseases. *PNAS Nexus*, 2(3), pgad038. <https://doi.org/10.1093/pnasnexus/pgad038>
- Read, J. A., Winter, V. J., Eszes, C. M., Sessions, R. B., & Brady, R. L. (2001). Structural basis for altered activity of M- and H-isozyme forms of human lactate dehydrogenase. *Proteins*, 43, 175–185. <https://doi.org/10.1002/1097-0134>
- Rinholm, J. E., Hamilton, N. B., Kessar, N., Richardson, W. D., Bergersen, L. H., & Attwell, D. (2011). Regulation of oligodendrocyte development and myelination by glucose and lactate. *The Journal of Neuroscience*, 31(2), 538–548. <https://doi.org/10.1523/JNEUROSCI.3516-10.2011>
- Ross, J. M., Öberg, J., Brené, S., Coppotelli, G., Terzioglu, M., Pernold, K., Gojny, M., Sitnikov, R., Kehr, J., Trifunovic, A., Larsson, N. G., Hoffer, B. J., & Olson, L. (2010). High brain lactate is a hallmark of aging and caused by a shift in the lactate dehydrogenase A/B ratio. *Proceedings of the National Academy of Sciences of the United States of*



- America, 107(46), 20087–20092. <https://doi.org/10.1073/PNAS.1008189107>
- Roth, J., Bendayan, M., & Orci, L. (1978). Ultrastructural localization of intracellular antigens by the use of protein A-gold complex. *The Journal of Histochemistry and Cytochemistry*, 26(12), 1074–1081. <https://doi.org/10.1177/26.12.366014>
- Saab, A. S., & Nave, K.-A. (2017). Myelin dynamics: Protecting and shaping neuronal functions. *Current Opinion in Neurobiology*, 47, 104–112. <https://doi.org/10.1016/j.conb.2017.09.013>
- Saab, A. S., Tzvetavona, I. D., Trevisiol, A., Baltan, S., Dibaj, P., Kusch, K., Möbius, W., Goetze, B., Jahn, H. M., Huang, W., Steffens, H., Schomburg, E. D., Pérez-Samartín, A., Pérez-Cerdá, F., Bakhtiari, D., Matute, C., Löwel, S., Griesinger, C., Hirrlinger, J., ... Nave, K. A. (2016). Oligodendroglial NMDA receptors regulate glucose import and axonal energy metabolism. *Neuron*, 91(1), 119–132. <https://doi.org/10.1016/J.NEURON.2016.05.016>
- Saito, T., Matsuba, Y., Mihira, N., Takano, J., Nilsson, P., Itoharu, S., Iwata, N., & Saido, T. C. (2014). Single app knock-in mouse models of Alzheimer's disease. *Nature Neuroscience*, 17(5), 661–663. <https://doi.org/10.1038/NN.3697>
- Sánchez-Abarca, L. I., Tabernero, A., & Medina, J. M. (2001). Oligodendrocytes use lactate as a source of energy and as a precursor of lipids. *Glia*, 36(3), 321–329. <https://doi.org/10.1002/GLIA.1119>
- Sato, T., Sayama, N., Inoue, M., Morita, A., & Miura, S. (2020). The enhancement of fat oxidation during the active phase and suppression of body weight gain in glycerol-3-phosphate dehydrogenase 1 deficient mice. *Bioscience, Biotechnology, and Biochemistry*, 84(11), 2367–2373. <https://doi.org/10.1080/09168451.2020.1792268>
- Sheppard, S., Santosa, E. K., Lau, C. M., Violante, S., Giovanelli, P., Kim, H., Cross, J. R., Li, M. O., & Sun, J. C. (2021). Lactate dehydrogenase A-dependent aerobic glycolysis promotes natural killer cell anti-viral and anti-tumor function. *Cell Reports*, 35(9), 109210. <https://doi.org/10.1016/j.celrep.2021.109210>
- Slot, J. W., & Geuze, H. J. (1985). A new method of preparing gold probes for multiple-labeling cytochemistry. *European Journal of Cell Biology*, 38(1), 87–93.
- Stumpf, S. K., Berghoff, S. A., Trevisiol, A., Spieth, L., Düking, T., Schneider, L. V., Schlaphoff, L., Dreha-Kulaczewski, S., Bley, A., Burfeind, D., Kusch, K., Mitkovski, M., Ruhwedel, T., Guder, P., Röhse, H., Denecke, J., Gärtner, J., Möbius, W., Nave, K.-A., & Saher, G. (2019). Ketogenic diet ameliorates axonal defects and promotes myelination in Pelizaeus-Merzbacher disease. *Acta Neuropathologica*, 138(1), 147–161. <https://doi.org/10.1007/s00401-019-01985-2>
- Suzuki, A., Stern, S. A., Bozdagi, O., Huntley, G. W., Walker, R. H., Magistretti, P. J., & Alberini, C. M. (2011). Astrocyte-neuron lactate transport is required for long-term memory formation. *Cell*, 144(5), 810–823. <https://doi.org/10.1016/j.cell.2011.02.018>
- Tognatta, R., Sun, W., Goebbels, S., Nave, K. A., Nishiyama, A., Schoch, S., Dimou, L., & Dietrich, D. (2017). Transient Cnp expression by early progenitors causes Cre-lox-based reporter lines to map profoundly different fates. *Glia*, 65(2), 342–359. <https://doi.org/10.1002/GLIA.23095>
- Trevisiol, A., Saab, A. S., Winkler, U., Marx, G., Imamura, H., Möbius, W., Kusch, K., Nave, K. A., & Hirrlinger, J. (2017). Monitoring ATP dynamics in electrically active white matter tracts. *eLife*, 6, e24241. <https://doi.org/10.7554/ELIFE.24241>
- Urbańska, K., & Orzechowski, A. (2019). Unappreciated role of LDHA and LDHB to control apoptosis and autophagy in tumor cells. *International Journal of Molecular Sciences*, 20(9), 2085. <https://doi.org/10.3390/IJMS20092085>
- Vajda, F., Jordi, N., Dalkara, D., Joly, S., Christ, F., Tews, B., Schwab, M. E., & Pernet, V. (2015). Cell type-specific Nogo-A gene ablation promotes axonal regeneration in the injured adult optic nerve. *Cell Death and Differentiation*, 22(2), 323–335. <https://doi.org/10.1038/CDD.2014.147>
- Valvona, C. J., Fillmore, H. L., Nunn, P. B., & Pilkington, G. J. (2016). The regulation and function of lactate dehydrogenase a: Therapeutic potential in brain tumor. *Brain Pathology (Zurich, Switzerland)*, 26(1), 3–17. <https://doi.org/10.1111/BPA.12299>
- Weil, M. T., Ruhwedel, T., Meschkat, M., Sadowski, B., & Möbius, W. (2019a). Transmission electron microscopy of oligodendrocytes and myelin. *Methods in Molecular Biology*, 1936, 343–375. https://doi.org/10.1007/978-1-4939-9072-6_20
- Weil, M. T., Schulz-Éberlin, G., Mukherjee, C., Kuo-Elsner, W. P., Schäfer, I., Müller, C., & Simons, M. (2019b). Isolation and culture of oligodendrocytes. *Methods in Molecular Biology*, 1936, 79–95. https://doi.org/10.1007/978-1-4939-9072-6_5
- Wyss, M. T., Jolivet, R., Buck, A., Magistretti, P. J., & Weber, B. (2011). In vivo evidence for lactate as a neuronal energy source. *The Journal of Neuroscience: The Official Journal of the Society for Neuroscience*, 31(20), 7477–7485. <https://doi.org/10.1523/JNEUROSCI.0415-11.2011>
- Ximerakis, M., Lipnick, S. L., Innes, B. T., Simmons, S. K., Adiconis, X., Dionne, D., Mayweather, B. A., Nguyen, L., Niziolek, Z., Ozek, C., Butty, V. L., Isserlin, R., Buchanan, S. M., Levine, S. S., Regev, A., Bader, G. D., Levin, J. Z., & Rubin, L. L. (2019). Single-cell transcriptomic profiling of the aging mouse brain. *Nature Neuroscience*, 22(10), 1696–1708. <https://doi.org/10.1038/S41593-019-0491-3>
- Yellen, G. (2018). Fueling thought: Management of glycolysis and oxidative phosphorylation in neuronal metabolism. *The Journal of Cell Biology*, 217(7), 2235–2246. <https://doi.org/10.1083/jcb.201803152>
- Zhou, W., Simic, P., Zhou, I. Y., Caravan, P., Vela Parada, X., Wen, D., Washington, O. L., Shvedova, M., Pierce, K. A., Clish, C. B., Mannstadt, M., Kobayashi, T., Wein, M. N., Jüppner, H., & Rhee, E. P. (2023). Kidney glycolysis serves as a mammalian phosphate sensor that maintains phosphate homeostasis. *The Journal of Clinical Investigation*, 133(8), e164610. <https://doi.org/10.1172/JCI164610>
- Zhou, Y., Song, W. M., Andhey, P. S., Swain, A., Levy, T., Miller, K. R., Poliani, P. L., Cominelli, M., Grover, S., Gilfillan, S., Cella, M., Ulland, T. K., Zaitsev, K., Miyashita, A., Ikeuchi, T., Sainouchi, M., Kakita, A., Bennett, D. A., Schneider, J. A., ... Colonna, M. (2020). Human and mouse single-nucleus transcriptomics reveal TREM2-dependent and TREM2-independent cellular responses in Alzheimer's disease. *Nature Medicine*, 26(1), 131–142. <https://doi.org/10.1038/S41591-019-0695-9>
- Zuend, M., Saab, A. S., Wyss, M. T., Ferrari, K. D., Hösl, L., Looser, Z. J., Stobart, J. L., Duran, J., Guinovart, J. J., Barros, L. F., & Weber, B. (2020). Arousal-induced cortical activity triggers lactate release from astrocytes. *Nature Metabolism*, 2(2), 179–191. <https://doi.org/10.1038/s42255-020-0170-4>

SUPPORTING INFORMATION

Additional supporting information can be found online in the Supporting Information section at the end of this article.

How to cite this article: Späte, E., Zhou, B., Sun, T., Kusch, K., Asadollahi, E., Siems, S. B., Depp, C., Werner, H. B., Saher, G., Hirrlinger, J., Möbius, W., Nave, K.-A., & Goebbels, S. (2024). Downregulated expression of lactate dehydrogenase in adult oligodendrocytes and its implication for the transfer of glycolysis products to axons. *Glia*, 1–18. <https://doi.org/10.1002/glia.24533>